EXPERIMENTAL STUDY OF SUPERCONDUCTING WIRE MOTION ON THE BASE INSULATING MATERIAL IN MAGNETIC FIELD

A Dissertation Submitted to
The Department of Accelerator Science,
School of High Energy Accelerator Science,
Graduate University for Advanced Studies, Japan
as a Partial Fulfillment of the Requirements for the Degree of
Doctor of Philosophy

Kailash Ruwali
2009

A Ph.D. Thesis

Experimental study of
superconducting wire motion on
the base insulating material in magnetic field

By
Kailash Ruwali

SUPERVISOR CERTIFICATE

This is to certify that the thesis entitled **"EXPERIMENTAL STUDY OF SUPERCONDUCTING WIRE MOTION ON THE BASE INSULATING MATERIAL IN MAGNETIC FIELD"** describes the original work done by **Kailash Ruwali**, under my supervision for the degree of **Doctor of Philosophy** of the Graduate University for Advanced Studies, Japan. Mr. Kailash Ruwali has fulfilled the required formalities as per the university rules known to us.

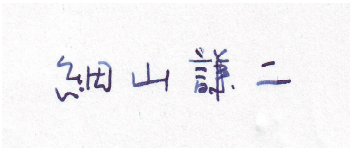

Prof. Kenji Hosoyama
Head, Cryogenics Division
KEK, Japan

Acknowledgement

I should like to express my appreciation to Dr. S.P. Mhaskar, who initially directed my attention to the field of magnets. My appreciation is also extended to each person at RRCAT, Indore, India, with whom I have been working since 1994. Special thanks to Prof. Shin-ichi Kurokawa for taking personal interest in my case and solving the visa problem for Indian Researchers (due to visa problem, I could not come to Japan in October 2004 to pursue my thesis work) which eventually made my stay as Doctoral student at KEK possible. Special thanks are due to Dr. P.D. Gupta, Director, RRCAT, Indore, India and Shri. Gurnam Singh, Head, IOAPDD, RRCAT, Indore, India for allowing me to pursue my thesis work at KEK, Japan.

I would like to express my deep gratitude to Prof. Kenji Hosoyama of KEK, Japan for accepting me as his graduated student and gave me an opportunity to study the superconducting wire motion in magnetic field. Prior coming to KEK, I have very little experience of working at cryogenic temperature. I would like to thank him for his valuable comments and suggestions in writing this thesis. I would like to thank him and Dr. Atsuhiko Yamanaka for their help in design and fabrication of experimental setup. Without their help and suggestions, it was impossible to complete this work in time.

I would like to thank Dr. Atsuhiko Yamanaka for preparing Zylon / Dyneema fiber based samples and also for carrying out their frictional coefficient measurement at room temperature at Toyobo Co. Ltd., Japan.

The support of Ministry of Education, Culture, Sports, Science and Technology (MEXT), Japan was certainly appreciated in granting me the scholarship.

A special word of appreciation is due to Dr. Kota Nakanishi for his help in handling enormous measurement data just before my final presentation of dissertation. At that time, I was running short of time and it is because of his timely help, I could finish my work in due course of time.

First of all, I want to thank my wife Meena for her warm encouragement, steady support and taking care of our kids Harshit and Tanishka during this three-year

gestation period of my thesis. Without her help it would not be possible for me to continue my work.

I would like to express my gratitude to my parents for their constant inspiration in learning science since my childhood. It is their motivation (especially my father, who happened to be a Plant Physiologist) by which I have chosen my career in research.

Thanks to my friends Dr. Randeep Rakwal, Anand Valecha, Subrata Das, Hari Vaswani, Navin Awale, Ashutosh Upadhayaya, Pramod R., Puneet Jain and Puneet Tyagi for their generosity and support they provided during my stay at KEK.

I am grateful to many individuals who have contributed to my education in magnets over the past years. I am indebted to Dr. Elwyn Baynham and Dr. Martin Wilson for many valuable comments and discussions.

The staff of KEK has been uniformly helpful and encouraging. I want especially to thank Mr. Yuuji Kojima for his help in conducting the experiments.

Working at KEK has strongly enriched my mind and character; for this reason I would like to thank all those people who made this experience possible, and helped me to successfully accomplish this work. My admiration is to Ms. Misa Miyai for her sincere cooperation.

Kailash Ruwali

THESIS
DEDICATED
TO
MY FAMILY

Especially to my wife Meena
for her consistent encouragement through out my Doctoral course.
She suffered a lot, staying alone in India and also in Japan but never complaint.

Everybody has difficult years, but a lot of times the difficult years end up being the greatest years of your whole entire life, if you survive them.
Brittany Murphy, *Seventeen Magazine, September 2003*

Summary

One of the most prominent applications of superconductivity is high field magnet. Mechanical disturbance such as abrupt conductor motion is one of the main origin of premature quench (transition from superconducting state to the normal resistive state) in high current density superconducting coils. The wire motion occurs when electromagnetic force to conductor exceeds constrain force including frictional force on the surface of conductor. Behavior of superconducting wire motion depends on the electromagnetic force acting on it, frictional property of the insulating material and thrust force applied to the superconducting wire.

The experiments for superconducting wire motion in magnetic field was carried out using small coil wound on stainless steel (SUS) bobbin using Polyimide film as an insulating material and high strength polyethylene fiber (Dyneema: DF) reinforced plastic (DFRP) bobbin [1]. The Dyneema fiber has negative thermal expansion [2] and low coefficient of friction [3]. It was found that voltage spikes generated due to sudden wire motion in case of DFRP bobbin are a few and small in amplitude. The speculations are; the negative thermal expansion of the DFRP bobbin restrains the wire motion and low coefficient of friction between superconducting wire and DFRP bobbin reduces sudden motion.

In order to study the effect of frictional coefficient of insulating material on superconducting wire motion under the influence of electromagnetic force, a special experimental setup was designed and fabricated. The main distinctiveness of the experimental setup is that the tension of the superconducting wire can be changed during the experiments. The experimental set up consists of a cryostat, superconducting solenoid magnet, sample holder, tensional unit to apply tension to the superconducting wire, power supplies and pen recorder or a 16-bit data recorder to measure the voltage tap signal. The sample holder consists of two parts, a semi-circular head and a body part. Experiments were conducted at 4.2 K by varying the experimental conditions such as the tension to the superconducting wire, superconducting wire current ramp rate and different insulating materials at the interface of the superconducting wire and semi-circular head.

Voltage taps to measure the signal generated due to the superconducting wire motion are connected at the end of the semi-circular head. To reduce the voltage tap loop area, a groove was incorporated in the semi-circular head and the voltage tap wire was passed through it. The voltage tap signal is measured by a pen recorder or a 16-bit data recorder with a sampling rate of 1 MS/s. Sudden wire motion was indicated by observing the voltage spikes.

In order to examine the effect of the current ramp rate on the superconducting wire motion, ramp rate was changed from 0.4 A/s to 1.69 A/s. The superconducting wire tension was varied from 7.1 N to 35.8 N to study the effect of tension on the superconducting wire motion. During all experiments, a constant magnetic field of 6 T was applied by superconducting solenoid magnet.

In the thesis work, different types of insulating material were used to study superconducting wire motion under electromagnetic force. They are Polyimide film, cloth / sheet material fabricated using Dyneema fiber, Zylon fiber and Teflon. The Dyneema / Zylon fiber has negative thermal expansion and a low coefficient of friction.

We have verified the effectiveness of this system. We could measure the pattern of voltage spikes. The time duration of voltage spikes are of the same order for all the samples. The peak voltage tap signal amplitude, velocity of wire motion, distance moved by wire and energy dissipated due to wire motion in case of Polyimide film is more than 2 order of magnitude larger than Dyneema based insulating materials and Zylon cloth. Hence use of Dyneema / Zylon based materials as an interface material between layers of superconducting wire may reduce the frictional heat generated due to wire motion and could make superconducting magnet performance more reliable.

List of publications by the candidate

The following is the list of external publications (i.e. the papers that are published in Journal, conference proceedings etc.) that are related to the research work described in this thesis.

1. "Stability of Superconducting Wire in Magnetic Field", K. Ruwali, A. Yamanaka, Y. Teramoto, K. Nakanishi, K. Hosoyama, in Proceedings of the 11th European Particle Accelerator Conference, Genoa, 2008 (EPS-AG, Genoa, Italy, 2008), p. 2449.

2. "Superconducting wire motion under the influence of electromagnetic force", K. Ruwali, A. Yamanaka, Y. Teramoto, K. Nakanishi, K. Hosoyama, in Proceedings of the Cryogenic Engineering Meeting, Autumn 2008 (In Japanese).

3. " Study of superconducting wire motion in magnetic field", K. Ruwali, A. Yamanaka, Y. Teramoto, K. Nakanishi, K. Hosoyama, in Proceedings of the 4th Indian Particle Accelerator Conference (InPAC2009), Indore, 2009.

4. "Experimental setup to detect superconducting wire motion", K. Ruwali, A. Yamanaka, Y. Teramoto, K. Nakanishi, K. Hosoyama, Phys. Rev. ST Accel. Beams 12, 042401 (2009).

5. "Dependence of superconducting wire motion on the base insulating material in magnetic field", K. Ruwali, A. Yamanaka, Y. Teramoto, K. Nakanishi, K. Hosoyama, Presented in PAC'09, Vancouver, Canada (Proc. To be published).

Contents

List of figures

List of tables

Chapter 1

Introduction

The aim of this chapter is to introduce the importance of study of the superconducting wire motion under the influence of electromagnetic force, principle of superconducting wire motion measurement, review of work carried out in the field of superconducting wire motion and organization of dissertation.

1.1 Superconducting Magnets

Superconducting magnets are now being used in variety of applications such as charge particle accelerators for High Energy Physics Research, Medical Resonance Imaging (MRI), Magnetic Levitation, Mossbauer Spectroscopy etc. Design and fabrication of superconducting magnets requires the highest quality of engineering.

The most outstanding feature of a superconducting magnet is its ability to support a very high current density with zero resistance while at the same time the operating costs are reduced. This characteristic permits magnets to be constructed that generate intense magnetic fields with little or no electrical power input. Since the current densities are high, superconducting magnet systems are quite compact and occupy only a small amount of laboratory space. Another feature of superconducting magnets is the stability of the magnetic field in the persistent mode of operation. In the persistent mode of operation, the time constant is extremely long and the magnet can be operated for days or even months at a nearly constant field.

Superconducting magnets are mostly intended for operation above 3 T, the superconducting coils primarily determine field shape. The two main design goals for superconducting magnets are to obtain a good quench performance (a quench implies the loss of superconductivity in the wire/cable) and a good field quality.

The superconducting state only exists when superconducting materials are maintained below the critical temperature. This temperature depends on the amount of current carried by the conductors and the magnetic field to which the conductor is subjected. A three-dimensional surface, called the critical surface, is defined by the

boundaries of critical temperature Tc, critical magnetic flux density Bc, and critical current density Jc, as shown in fig. 1.1. Superconductivity vanishes for any set of two parameters, if the third parameter increases beyond the critical surface. This transition process where the superconductor changes from the superconducting state to the normal resistive state is called quench. Quenches below the expected maximum quench current have at least four origins:

(1) Energy deposition in the magnet coil resulting from frictional motions under the Lorentz force.

(2) Energy deposition from beam losses.

(3) Heat dissipation from coupling currents in the cable.

(4) Current imbalances among cable strands.

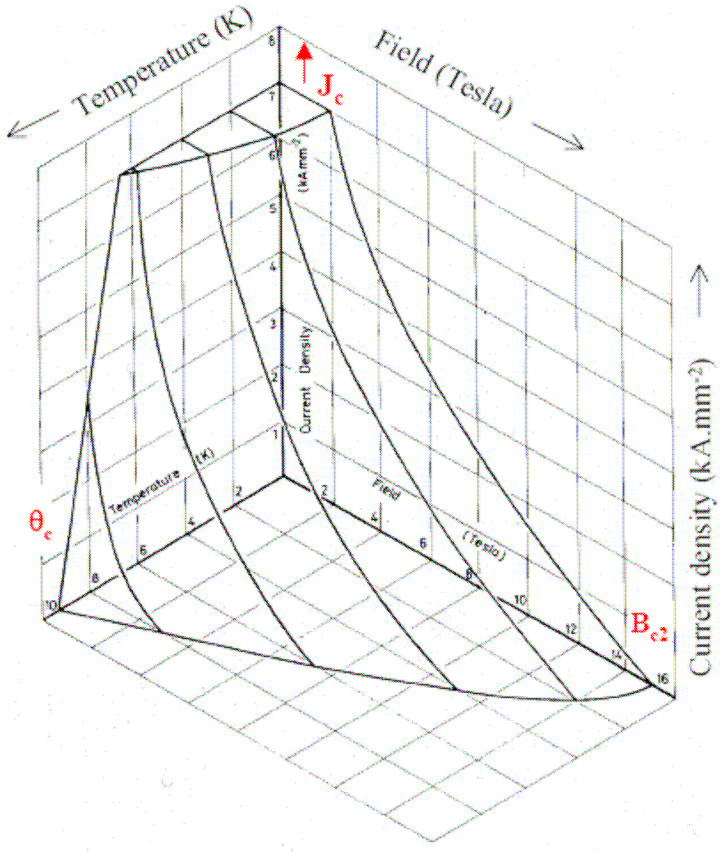

Figure 1.1: Superconducting/resistive phase transition surface of niobium-titanium.

Quenches of the first origin are revealing of flaws in the mechanical design or in the assembly procedures, which must be analyzed and corrected.

Good quench performance of the superconducting magnets is closely related to a good mechanical design, which minimizes the motion of the superconducting wires. The design must be structurally sound to deal with the Lorentz forces when the magnet is energized, the thermal forces during cool down of the magnet.

There exists 2 types of superconductors namely; cryostatically stabilized conductors and finely subdivided conductor (filamentary composite wires). The fully stabilized conductors have such a large copper cross section and which is so well cooled by being in good contact with the helium refrigerant that it can carry the rated current without the temperature rising unduly. Following a disturbance current shared between copper and superconductor, ohmic heat generation is transferred to the coolant and when available cooling exceeds heat generation, temperature falls and current returns to the superconductor. Schematic view of operation of cryostatically stabilized conductors is shown in fig. 1.2. The final temperature tolerable depends on detail considerations but is of the order of the critical temperature. The analysis has been reviewed and extended by Maddock *et* al [4]. If the superconductor does go normal the current transfers to the copper until such time (the thermal diffusion time, possibly only fractions of a second) as the superconductor recovers. The design of conductors of this type has been discussed by Maddock and James [5]. Using this technique a number of large coils have now been operated successfully [6, 7, 8]. Despite this, there are a number of disadvantages. First, it is difficult to change the field rapidly without causing large energy losses (both eddy current in the copper, and

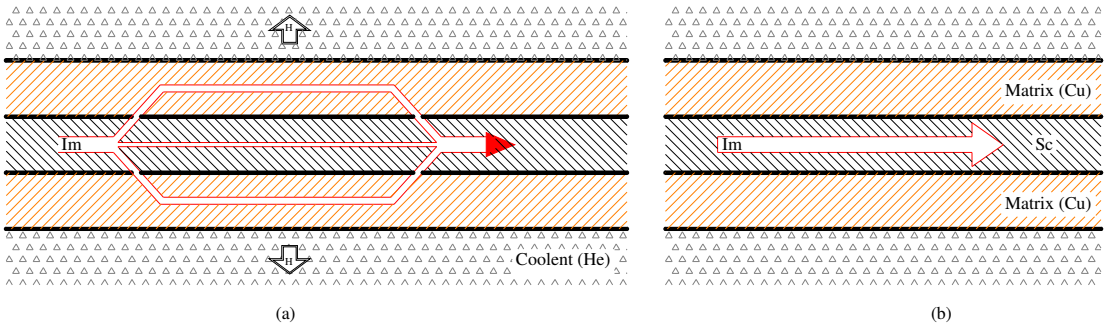

Figure 1.2: Schematic view of operation of cryostatically stabilized conductor.

hysteresis in the superconductor in the forms first developed) and so driving the coil normal; secondly, the optimum design of conductor is different for each coil, thus leading to high manufacturing costs, and thirdly, the coil design is considerably complicated by the need to provide many helium ducts. As these difficulties are avoided in the alternative conductors, full stabilization is now largely obsolete.

Most superconducting magnets are wound using conductors, which are comprised of many fine filaments of a niobium-titanium (NbTi) alloy embedded in a copper matrix. NbTi had good mechanical properties (ductility) but is generally limited to producing ~7.5 T at 4.5 K and ~10.5 T at 1.8 K. The Titanium in NbTi alloy is generally about 46% by weight. The coils are kept below a temperature of 4.2 K inside a cryostat. The cryogenic system is designed to minimize the heat leak to room temperature outside the cryostat.

Superconducting magnet coils fabricated using finely subdivided conductors are stable against flux jumping (the sudden and dissipative rearrangement of magnetic flux within a superconductor) [9] but are subjected to mechanical disturbances, which are the major cause for the premature quench. Mechanical disturbances such as conductor motion caused by the Lorentz force on the conductor in the magnet are the dominant source of degradation in the performance of high current density magnets and a major cause for concern in the design of very large high magnetic field systems [10]. Because of the very low heat capacities and the very high stresses, which can be set up, movements of only a few micrometers may theoretically be sufficient to trigger off a quench. Quenching at lower currents than the critical current is generally known as degradation. It is often accompanied by a related behavior known as training. After successive quenches, the magnet is able to achieve progressively higher currents. To avoid this training effect, it is necessary that the conductors be securely bonded in place to prevent them from moving.

In practical magnets, it is impossible to wind coils which fit together snugly at the micron level and the problem of wire movements has therefore been tackle by impregnating the coil with resins or waxes which fill all the remaining spaces. Impregnation has been very successful in reducing wire motion and is now standard practice in magnet construction. Even in the impregnanted magnet, training is one of

the major concern. Unfortunately, the resin contracts much more than the metal, so it goes into tension. Furthermore, almost all organic materials become brittle at low temperature. The use of organic impregnates can introduce other kinds of energy disturbance. A plausible explanation of the long training sequences generally displayed by resin-impregnated magnet is that, during the training process, all those places, which must crack, are cracking. Once the cracking has happened, the coil is "trained" and able to reach higher currents before quenching. Wire motions in the magnetic field, cracking epoxy, and eddy currents generate heat.

1.2 Superconducting wire motion under the influence of electromagnetic force

Superconducting wire motion under the influence of electromagnetic force (Lorentz force) are the main cause of premature quench in high performance and high current density superconducting magnets [11, 12]. In the first approximation, Lorentz force is proportional to B^2

$$\vec{F} = \vec{I} \times \vec{B} \, \alpha \, B^2$$

and is extremely high in high-field magnets.

Accelerator magnets are operated close to the critical current limit (~ 90% of critical current) of their wire / cables, the electromagnetic work produced by minute wire motions in the coils are of the same order of magnitude as the energy depositions needed to trigger a quench [13]. During the excitation of the superconducting coil, the wires / strands are subjected to strong Lorentz forces, which induce shear stress at the metal / metal and metal / insulation interfaces. The later is considered to be the largest and potentially most harmful source of frictional heating. Hence, frictional properties on contacting combinations of the superconducting wire and winding structures are important parameters for characterizing stability of the superconducting windings. Kinsley and Iwasa [14] have made a detailed study to observe sliding behavior at 4.2 K, 77 K and 295 K for a number of polymers, laminated composites and coated pieces sliding against either copper or aluminum. They found that, some surfaces

show stick-slip friction with sudden release of energy, some slide gradually in a stable fashion and therefore release the stored energy quite slowly.

This leaves two possibilities; either to prevent wire or coil motions by providing a rigid support against the various components of the Lorentz force or to reduce to a minimum the friction coefficients between potentially moving parts of magnet assembly [15]. In the superconducting magnets used for accelerator, in the radial direction; the coils are confined by laminated collars, which are locked around the coils by means of keys or tie rods as shown in fig.1.3 [16]. In the azimuthal direction; the collars are assembled so as to pre-compress the coils. In the axial direction; the coils either are free to expand or are restrained by means of stiff end plates. Figure 1.4 shows the magnitude of the components of the individual turns in a SSC 50 mm prototype dipole magnet [16]. The radial component of the force (F_r) pushes the coil outward and the azimuthal component (F_a) compresses the coil towards the midplane (horizontal plane).

In order to study the effect of the frictional coefficient of insulating material on the superconducting wire motion under the influence of electromagnetic force, a special experimental set up was designed and fabricated. The main distinctiveness of the experimental set up is that the tension of the superconducting wire can be changed during the experiments.

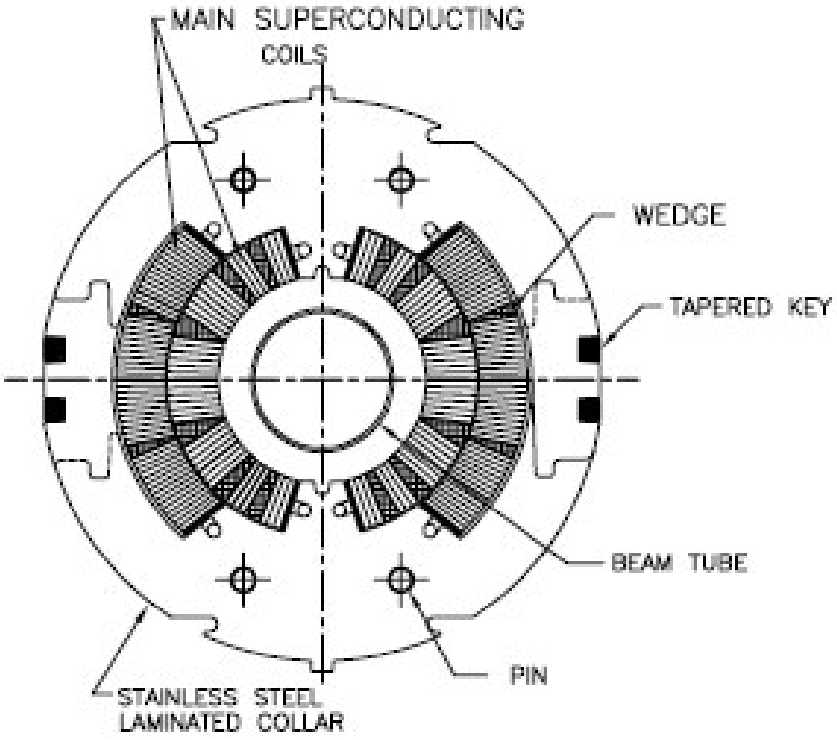

Figure 1.3: Cross-section of the optimized coil for the prototype SCC 50 mm main collider dipole magnet.

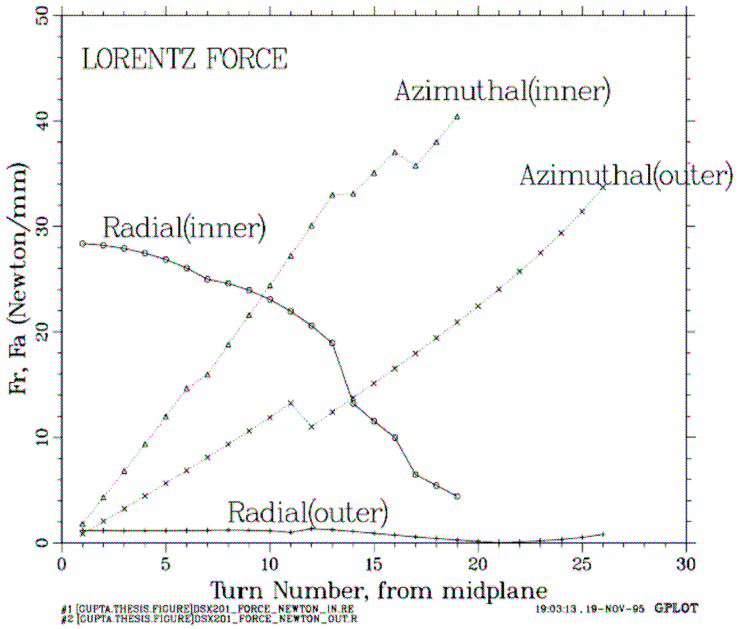

Figure 1.4: Magnitude of the components of the Lorentz force on the individual turns in a SCC 50 mm prototype magnet.

1.3 Review of wire motion studies and motivation

In superconducting magnets, due to strong electromagnetic force, wire motions took place and are primarily responsible for the quench. Comprehensive solution to obtain the stable superconducting magnets has not been found out yet.

Direct experimental observations on the instabilities caused by mechanical disturbances, which includes friction between superconductors or between superconductor and insulator are few [9]. However, several studies have been reported on the frictional disturbance resulted from wire motion [9, 15, 17, 18, 19].

Direct observation of the emf induced by wire motion and disturbance energy released by wire motion caused by electromagnetic forces in quadrupole magnet for TRISTAN Main Ring reported elsewhere [13, 20]. Later on, a theoretical model for simulation of wire movement in a superconducting coil was proposed by Nishijima et al [21]. In the proposed model, solving the equation of motion of each winding, frictional heat generated was estimated and quench current was derived. Shimizu et al [22] proposed a theoretical model to incorporate the mechanical instabilities in a.c. Nb-Ti superconducting wire.

The experiments on superconducting wire motion [1] in the magnetic field were carried out using small coils wound on stainless steel (SUS) bobbin with Polyimide film as the insulating material and also with high strength polyethylene fiber (Dyneema DF) reinforced plastic (DFRP) bobbins. The Dyneema fiber has negative thermal expansion [2] and a low coefficient of friction [3]. Each completed coil had one layer and 39 turns. The sample coil is inserted in the superconducting solenoid magnet as shown in fig. 1.5. Voltage tap wire is connected at both ends of the sample coil. The sample coil voltage was measured during current ramp up in constant magnetic field provided by the superconducting solenoid magnet. Figure 1.6 shows the induced voltage and excitation current of SUS and DFRP bobbin. The conductor on SUS bobbin moves easily and quickly. The wire motions of the conductor on DFRP bobbin have been constrained by the bobbin. The induced voltages between both ends of the sample coils during excitation show some sharp peaks for the coil of SUS bobbin in 5-6 T, but those for DFRP bobbin has only a few

small peaks. The speculations for low amplitude and a few voltage spikes are as follows; the negative thermal expansion of the DFRP bobbin restrains the wire motion and the low coefficient of friction between superconducting wire and DFRP bobbin reduces sudden motion.

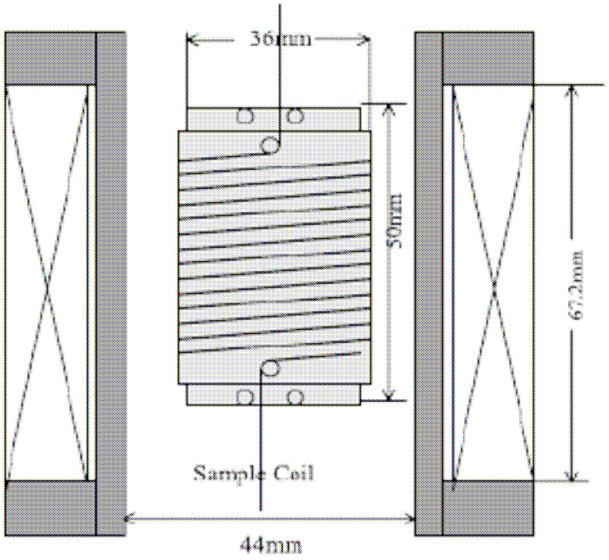

Figure 1.5: Schematic illustration of sample coil and back up coil.

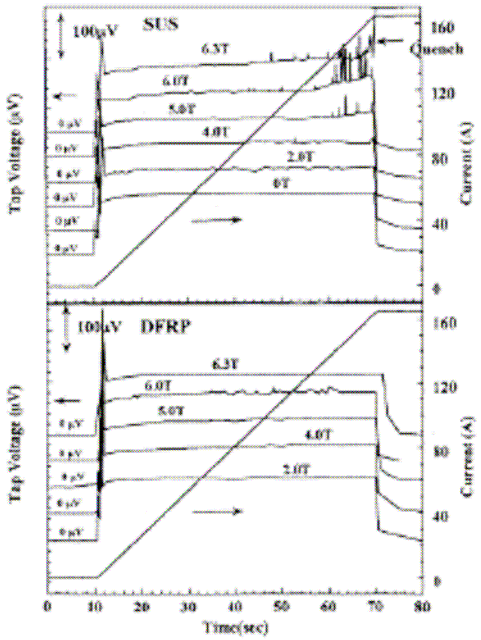

Fig. 1.6: Induced voltage and excitation current of SUS and DFRP bobbin.

1.4 Principle of superconducting wire motion

The working principle of superconducting wire motion under the influence of electromagnetic force is based on the Lorentz force experienced by the superconducting wire and is shown in fig. 1.7. The superconducting wire is set on the semi-circular head of the radius 18 mm and the tension T of the superconducting wire provides a uniform thrust force F_t (of the superconducting wire) against the semi-circular head as shown in fig. 1.8. The relation between the thrust force per unit length is (see Appendix I)

$$F_t = T/r$$

where, r = radius of semi-circular head.

The current $\vec{I}$ is fed to the superconducting wire using an external power supply and the superconducting solenoid magnet provides the magnetic field. Voltage tap to measure the signal due to the superconducting wire motion are connected at the

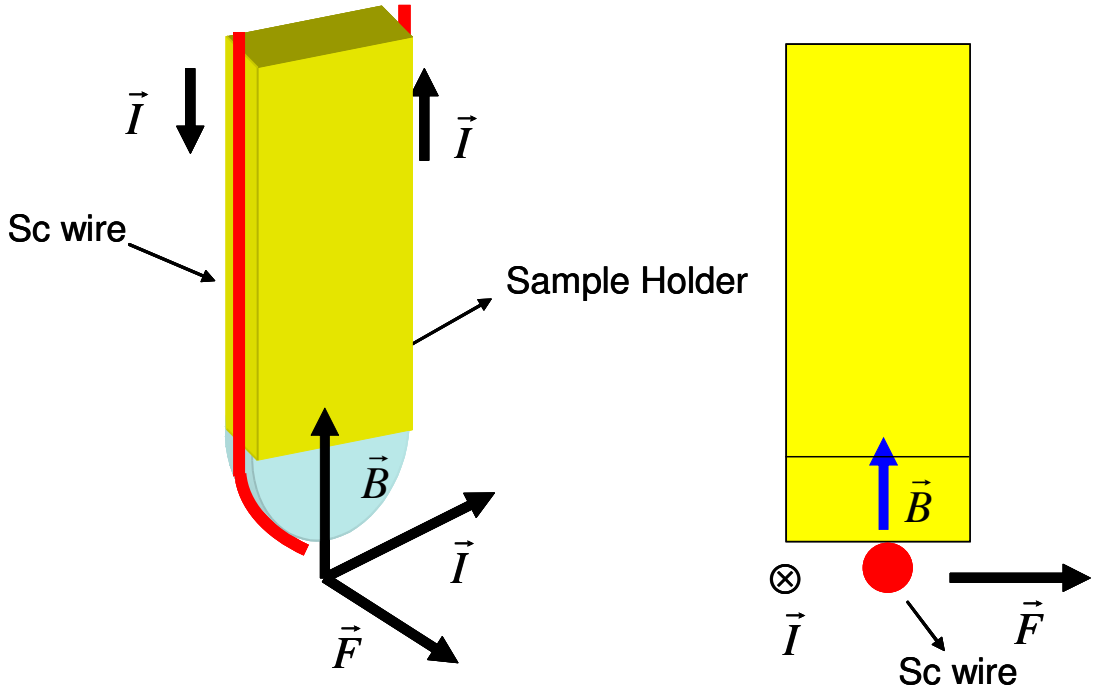

Figure 1.7: Working principle of the experimental setup.

end of the semi-circular head. Sudden wire motion was indicated by observing the voltage spikes.

The Lorentz force per unit length of the superconducting wire is given as

$$\vec{F} = \vec{I} \times \vec{H} = IHSin\,\theta = IH$$
$$when\,, \theta = 90°$$

The maximum Lorentz force on the superconducting wire is at the bottom of semi-circular head. It is predicted that the wire motion starts from there, when the Lorentz force exceeds frictional force. View of forces acting on the surface of superconducting wire is shown in fig. 1.9. The wire then moves for a small distance before being stopped by frictional force.

Figure 1.10 shows the measurement principle. It is expected that wire motion will occur during the current ramp in superconducting wire due to electromagnetic force. On subsequent ramp, amplitude of voltage generated due to wire motion will reduce and also less number of voltage spikes will be detected.

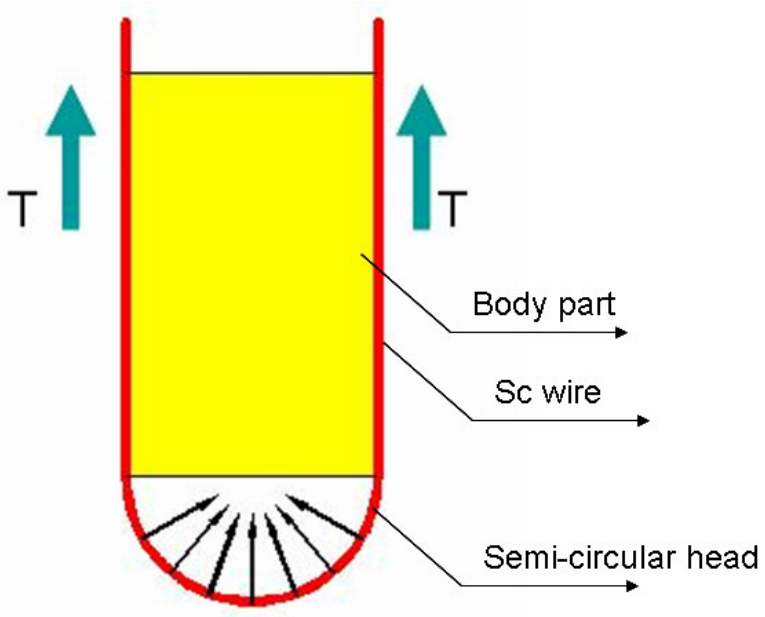

Figure 1.8: Thrust force applied by the superconducting wire to the semi-circular head.

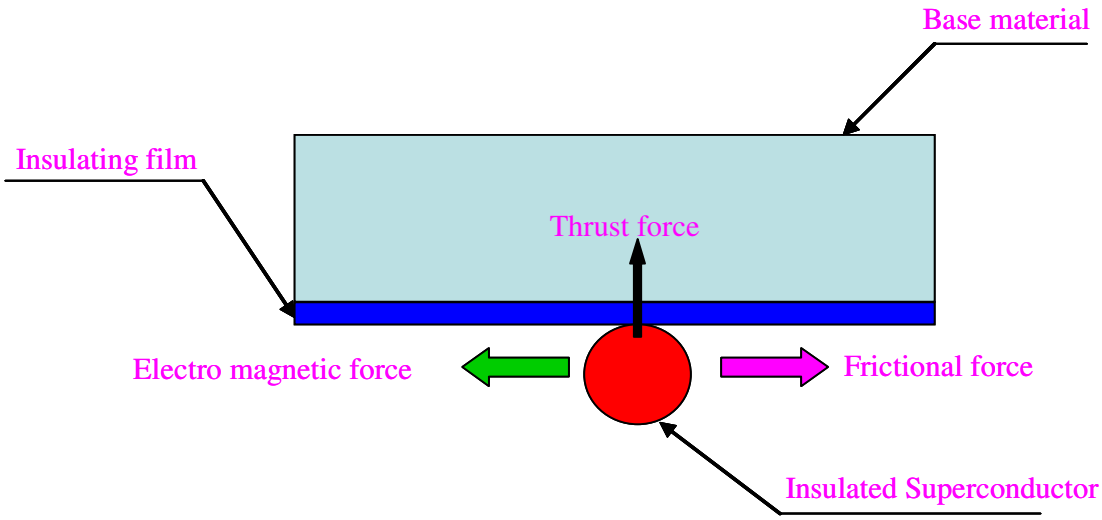

Figure 1.9: View of forces acting on superconducting wire.

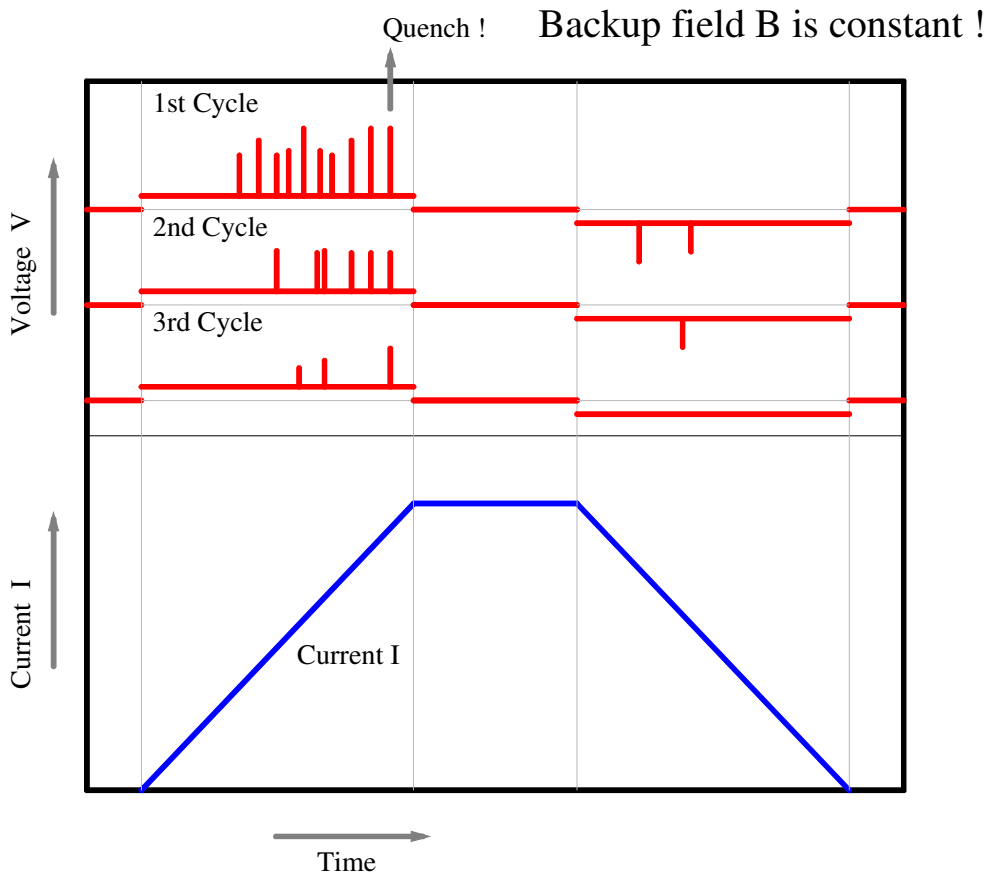

Figure 1.10: Measurement principle of wire motion experiment.

1.5 Objective of our study

The main aim of present research work is

(1) Design and development of an experimental setup to detect superconducting wire motion.

(2) To study the time dependence profile of wire motion.

(3) To study the dependence of superconducting wire motion on:

- (i) coefficient of friction of insulating material
- (ii) applied tension to the superconducting wire
- (iii) current ramp rate
- (iv) current polarity

A special experimental set up was designed and fabricated to study the effect of the frictional coefficient of insulating material on the superconducting wire motion under the influence of electromagnetic force. The experimental set up consists of a cryostat, superconducting solenoid magnet, sample holder, tensional unit to apply tension to the superconducting wire, power supplies and pen recorder or a 16-bit data recorder to measure the voltage tap signal. The main distinctiveness of the experimental setup is that the tension of the superconducting wire can be changed during the experiments.

Superconducting wire motion depends on the electromagnetic force acting on it and frictional property of the insulating material. If the coefficient of friction of the insulating material is low, then one expects smooth and many wire motions. During this process, the energy will be released quite smoothly. On the contrary, if the coefficient of friction of insulating material is high, then one expects sudden and less number of wire motions with a sudden release in the energy. Hence, frictional properties of the conductors and winding structures are important parameters for characterizing stability of the superconducting windings.

Experiments were carried out at 4.2 K to study the superconducting wire motion under different experimental conditions such as; different insulating material at the interface of superconducting wire and semi-circular head, varying the tension to the superconducting wire, varying the current ramp rate and varying the

electromagnetic force. The insulating materials which are commonly used in high field superconducting magnets are taken for study such as Polyimide film, Teflon, Zylon cloth and Dyneema based materials.

1.6 Organization of dissertation

An overview of the superconducting wire motion measurement principle under the influence of electromagnetic force, review of work in wire motion studies and objective of our study are described in previous sections. Chapter 2 introduces the experimental equipments, measurement technique and properties of insulating materials used during experiments. Experimental procedure and findings during the course of thesis work are illustrated in Chapter 3. Conclusions drawn during the course work and further work to be carried out are discussed in Chapter 4.

Chapter 2

Experimental setup to detect wire motion

Design details of the experimental setup and instruments used to measure the superconducting wire motion under the influence of electromagnetic force are described in this chapter. Superconducting wire motion depends on the frictional property of the insulating material, tension applied to the superconducting wire and electromagnetic force experienced by the superconducting wire. Generally, a coating of insulating material is applied to the base material before the start of coil winding, between the coil layers, after completion of coil and as a spacer. Some of the commonly used insulating materials such as Polyimide film, Teflon, Zylon Cloth and Dyneema based materials are taken for the study. The properties of materials that were used during the experiments are also discussed in this chapter.

2.1 Experimental setup

The experimental setup consists of a cryostat, superconducting solenoid magnet, sample holder, tensional unit to apply tension to the superconducting wire, power supplies and pen recorder or a 16-bit data recorder to measure the voltage tap signal. Schematic view of the experimental setup is shown in fig. 2.1. In order to save the cost and time, we used the cryostat and superconducting solenoid magnet, which were readily available with KEK Crab Cavity Group. The details of sub-systems are described in following sub-sections.

2.1.1 Cryostat

Vertical cryostat of 200 mm in diameter and 1250 mm in height was used for the experiments. It consists of two vessels; the inner one for cooling the superconducting magnet with liquid helium and the outer one for providing the heat sink of 80 K thermal shield with liquid nitrogen. The thermal shields are placed between the liquid helium vessel and the external housing, which are wrapped with multi layered super insulation. The inner vessel is made of cryogenically compatible

low-carbon steel (SS-316L), especially for its property of very good weldability and the outer vessel is made of SS-304. The thermal load to LHe is 0.73 W, equivalent to the LHe evaporation rate of 1.5 L/Hr with superconducting solenoid magnet.

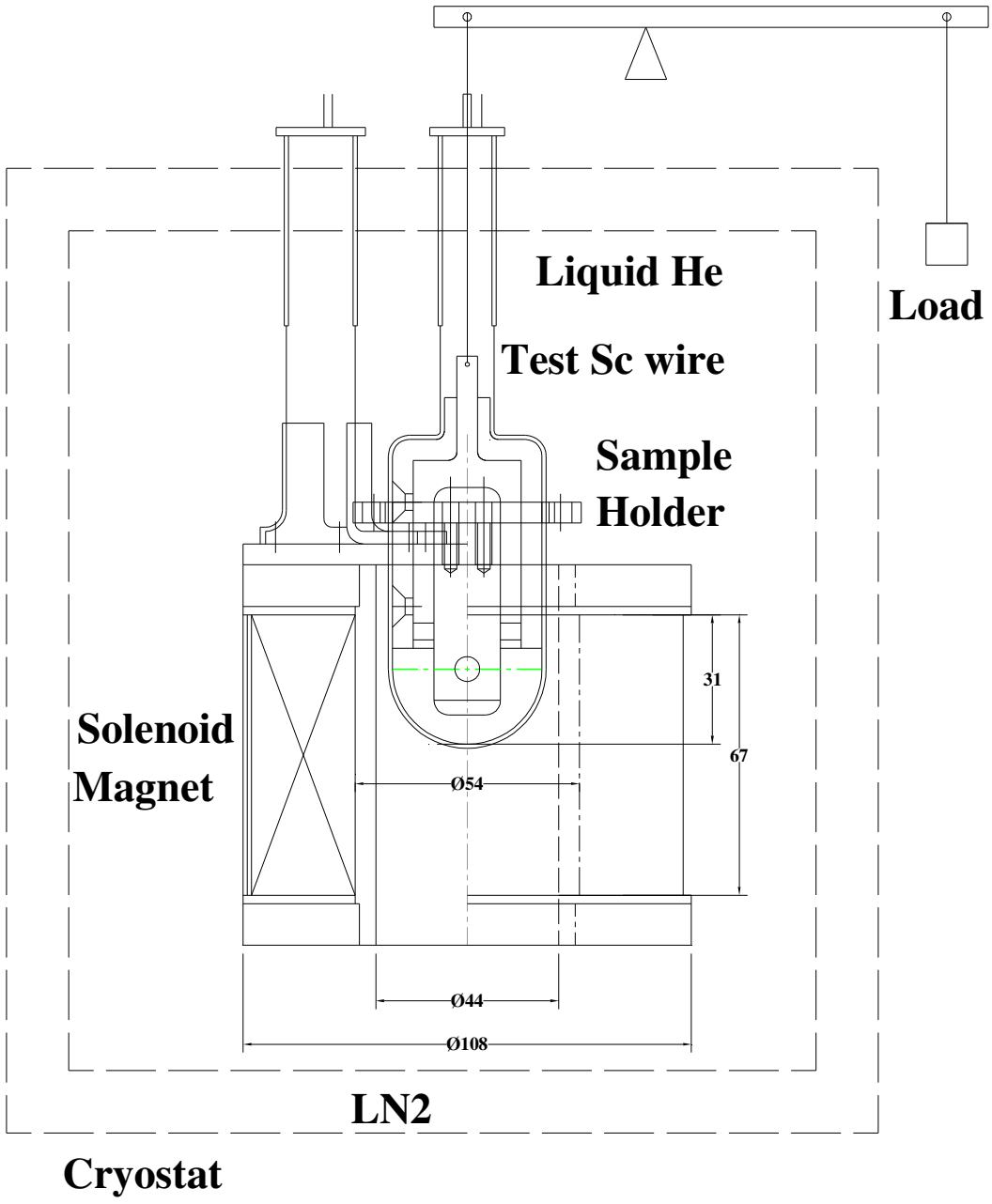

Figure 2.1: Schematic view of experimental set up.

2.1.2 Solenoid Magnet

Superconducting solenoid magnet can provide a magnetic field of 7 T at 148 A. The inner and outer diameter of the magnet is 54 mm and 103 mm respectively. The length of magnet is 67.5 mm. Main parameters of superconducting solenoid magnet are given in table 2.1. It is wound using NbTi superconducting wire and the characteristics of superconducting wire are given in table 2.2.

Table 2.1: Specification of superconducting solenoid magnet

Parameter	Value
Designed magnetic field	7 T
Inner/Outer diameter	54/103 mm
Total no. of turns	3839
Current @ 7 T	148 A
Length of magnet	67.5 mm
Inductance	0.65 H

Table 2.2: Specification of superconducting wire

Parameter	Value
Material	NbTi in copper matrix
Wire diameter	0.7 mm
Insulation	Formvar
Insulation thickness	~ 10 μm
No. of filaments	~ 10,000
Filament diameter	6 μm
Twist pitch	30 mm
NbTi/Cu	1:1.8
Ic	383 A @ 4T 260 A @ 6 T 100 A @ 8.57 T

2.1.3 Sample Holder

The sample holder shown in fig. 2.2 consists of two parts; a semi-circular head of radius 18 mm fabricated using SS316 L and a body part fabricated using G-10. Dimensions of the superconducting solenoid magnet were taken as a reference for the design of sample holder. The superconducting wire is wound on the semi-circular head and soldered to the copper terminals. The semi-circular head is installed and fixed to the superconducting solenoid magnet using support bars. The body part can move upward to change the tension of the superconducting wire. Insulating material is inserted between the semi-circular head and the superconducting wire. Voltage taps to measure the signal due to the superconducting wire motion are connected at the end of semi-circular head. To reduce the voltage tap loop area, a groove was incorporated in the semi-circular head as shown in fig. 2.3 and the voltage tap wire was passed through it. In order to reduce the noise and thermoelectric voltage, enameled copper wire (Φ 0.2 mm) was twisted and is directly connected to pen recorder / data recorder. Figure 2.4 shows the picture of sample holder placed inside the aperture of superconducting solenoid magnet.

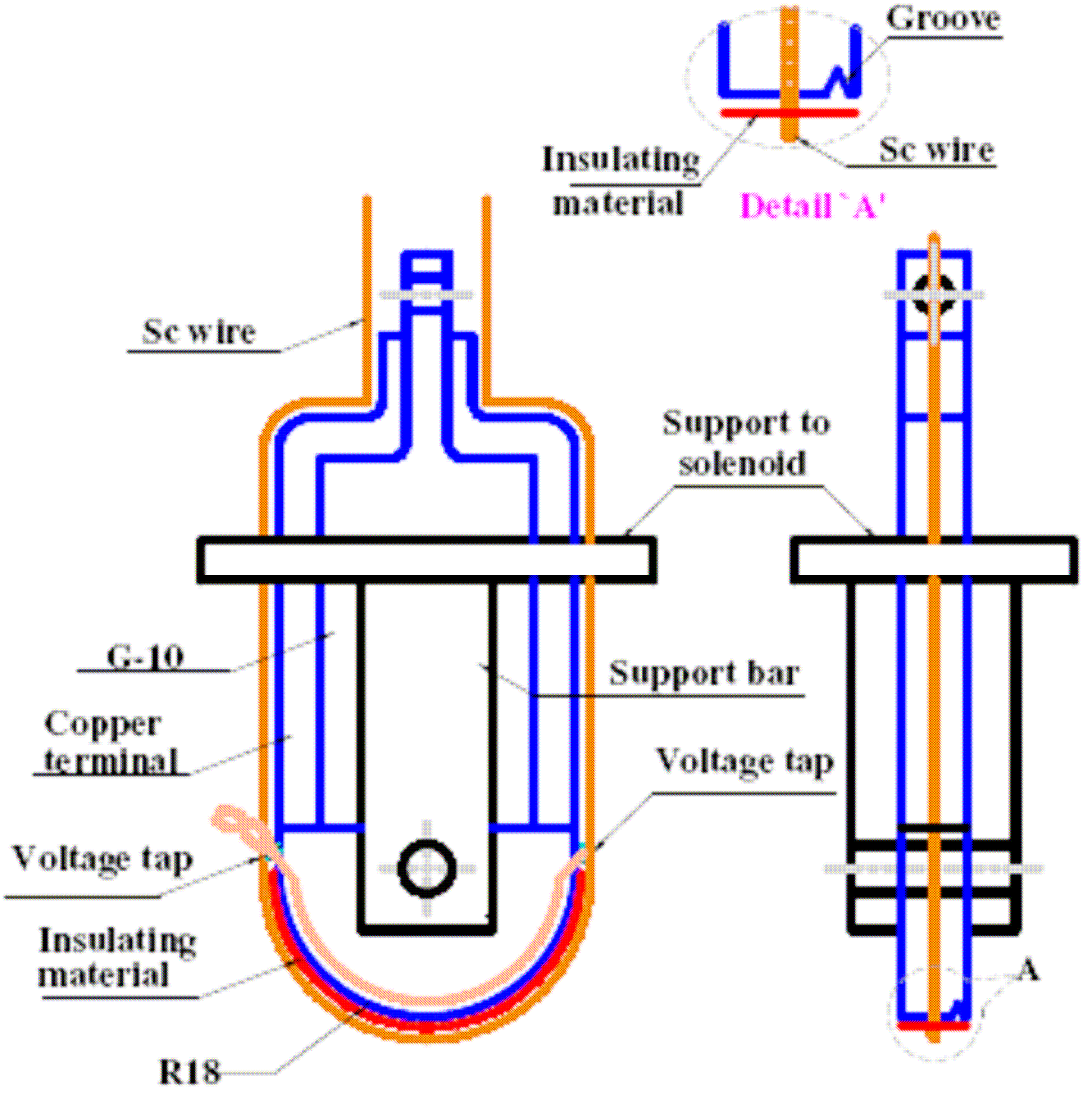

Figure 2.2: Schematic view of sample holder.

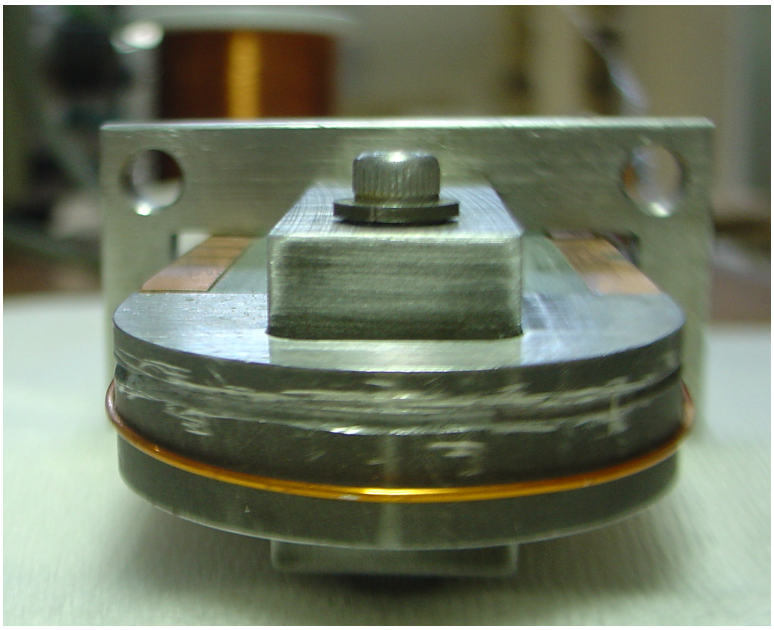

Figure 2.3: Picture showing groove incorporated in the semi-circular head part of the sample holder.

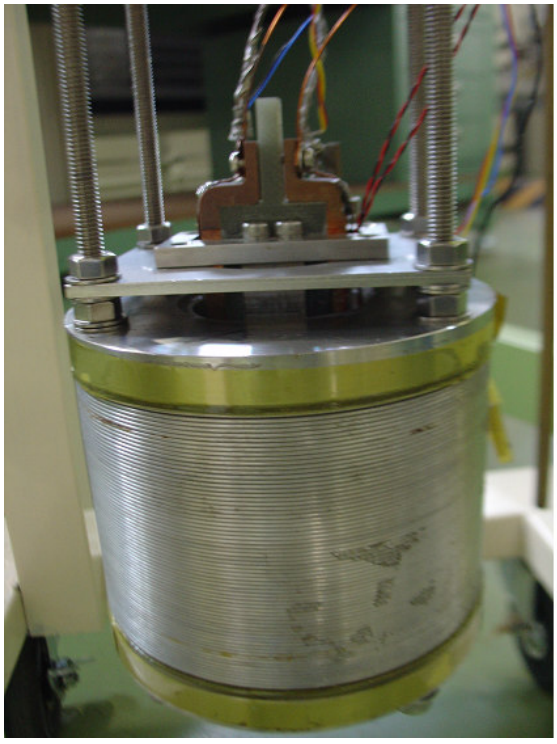

Figure 2.4: Picture showing sample holder sitting inside solenoid magnet.

2.1.4 Superconducting wire

The superconducting wire was made of NbTi filaments in a copper matrix with formvar insulation. The copper-to-superconductor ratio is 1.8 and the filament diameter is 6 μm. Other characteristics of wire are given in table 2.2. Figure 2.5 shows the typical current density for NbTi superconductor at 4.2 K and 1.8 K [23].

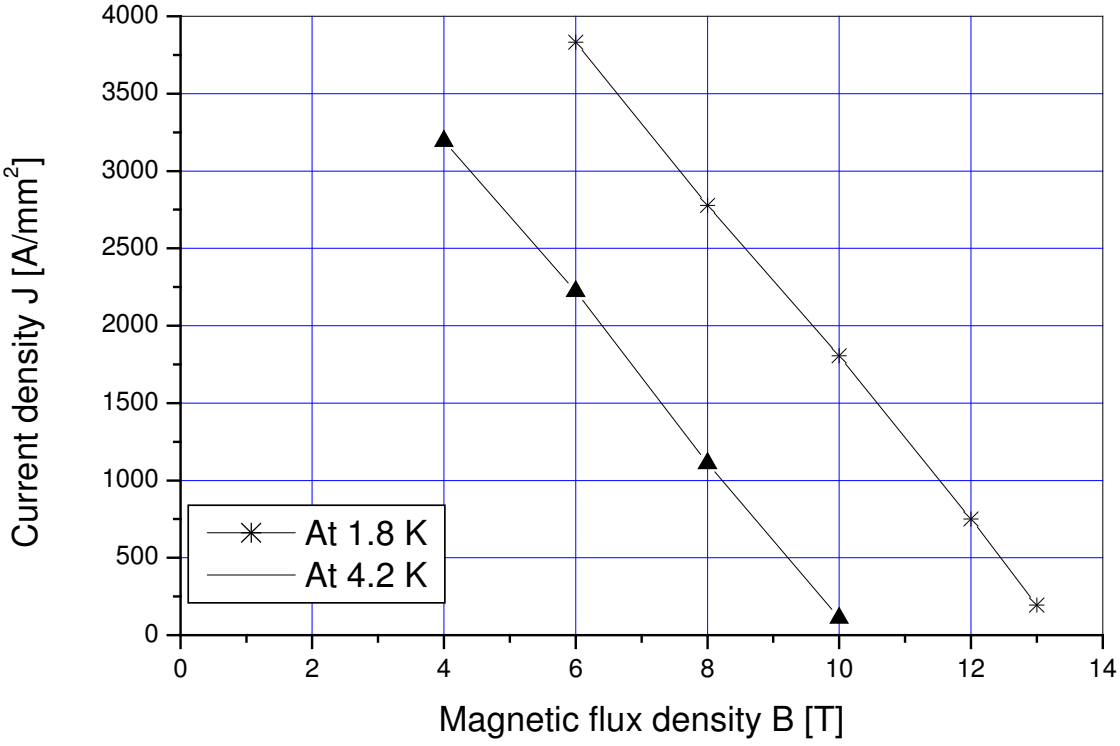

Figure 2.5: Typical current densities of NbTi superconductor.

2.1.5 Tensional Unit

In order to apply tension to the superconducting wire, a string is attached to the body part of the sample holder from the top flange and tension is applied via lever mechanism. The tension of the superconducting wire provides a uniform thrust force to the semi-circular head part as shown in fig. 1.5. The tension can be varied as per requirement by adjusting the load. The superconducting wire tension was varied from 7.1 N to 35.8 N to study the effect of tension on the superconducting wire motion under the influence of electromagnetic force.

During the winding of superconducting solenoid magnet which was used during the experiments, tension of 29.4 N was applied to the superconducting wire.

2.1.6 Instrumentation

Programmable power supplies (6V, 160A) were used to feed the current to the superconducting solenoid magnet and the superconducting wire. Current in the solenoid magnet was fixed (120 A) while the current in the superconducting wire was ramped from 0 A to 118 A. The current ramp up and ramp down rate was 0.85 A/s with a flat top of 60s. In order to examine the effect of the current ramp rate on the superconducting wire motion, the current ramp rate was changed from 0.4 A/s to 1.69 A/s. Voltage taps to measured the signal due to the superconducting wire motion are connect at the end of the semi-circular head. The voltage tap signal is measured by a pen recorder [24] or a 16-bit data recorder with a sampling rate of 1MS/s [25].

Liquid helium level sensor is installed to measure the helium level in the cryostat.

2.2 Insulating Materials

Insulating material is used at the interface of former and insulated superconducting wire, between the coil layers, after completion of coil and as a spacer. The main requirements for insulating materials are listed below [26]:

(1) Good dielectric strength in helium environment and under high transverse pressure (up to 100 Mpa).
(2) Small thickness (to maximize overall current density in magnet coil) and good physical uniformity (to ensure proper conductor positioning for field quality).
(3) Retention of mechanical properties in a wide temperature range.
(4) Ability to withstand radiations in an accelerator environment.

In addition, the insulation system is required to provide a means of bonding the coil turns together to give the coil a rigid shape and facilitate its manipulation during the subsequent steps of magnet assembly. Note that the dielectric strength of helium gas at 4.2 K is far worse than that of liquid helium and that it degrades significantly with increasing temperature [27].

In the thesis work, Polyimide film, Teflon, Zylon cloth and Dyneema based insulating materials are taken for the study. Frictional coefficient measurement of samples were carried out at room temperature at Toyobo Co. Ltd., Japan. Figure 2.6 shows the schematic view of experimental set up used for the frictional coefficient measurement. The measured values are given in table 2.3. Figure 2.7 shows the typical plot of measured frictional coefficient in case of Polyimide film. The properties of these materials are discussed in next sub sections.

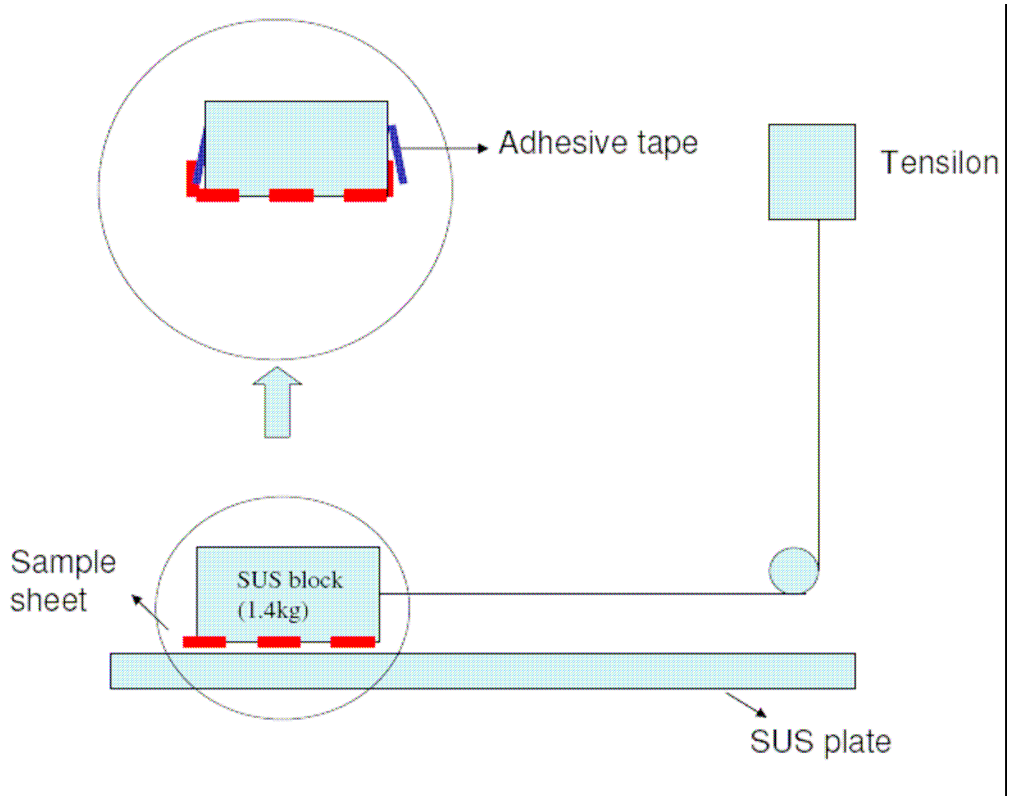

Figure 2.6: Schematic view of experimental set up used for the frictional coefficient measurement at room temperature.

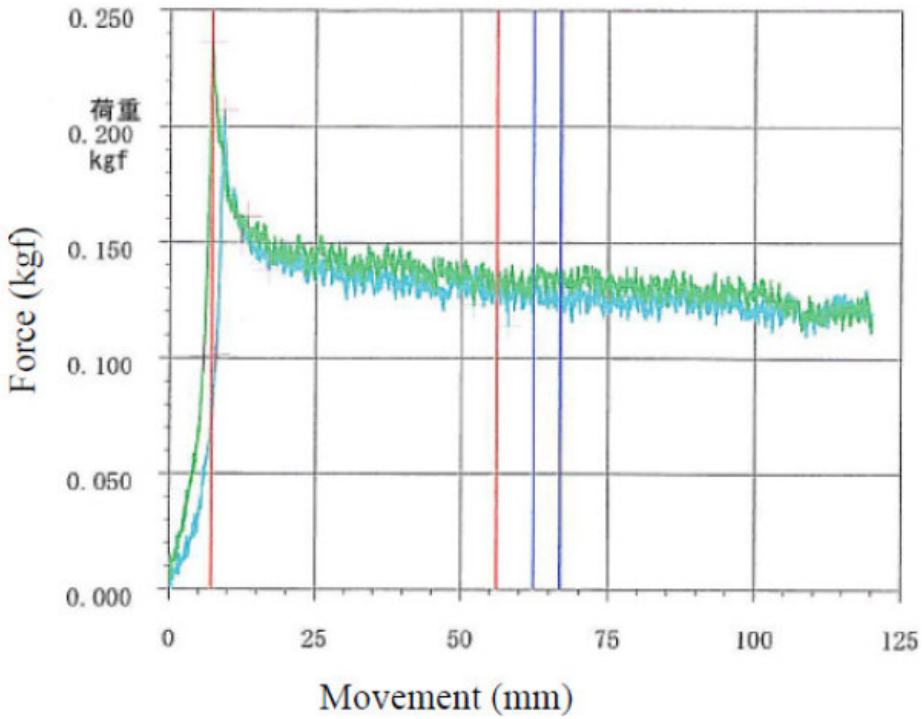

Figure 2.7: Frictional measurements plot in case of Polyimide film.

Table 2.3: Measured frictional coefficient at room temperature

Sample	Frictional coefficient	
	Static	Moving
Polyimide Film	0.1932	0.1401
Dyneema Cloth Sheet	0.1015	0.055
Dyneema non-woven sheet	0.145	0.074
Dyneema random sheet	0.147	0.129
Zylon Cloth Sheet	0.153	0.127
Teflon (Not measured)	Quoted in the range of 0.05 to 0.2	

2.2.1 Polyimide film

Polyimide film posses unique combinations of properties that make it deal for a variety of applications in many different industries. It maintains its excellent physical, electrical, and mechanical properties over a wide temperature range. It is synthesized by polymerizing an aromatic diahydride and an aromatic diamine.

Polyimide film is commonly used insulating material in high field superconducting magnets and also for room temperature electromagnets. The insulation of Tevatron, HERA magnets, SSC magnets and LHC magnets are constituted of one or two inner layers of Polyimide film, wrapped helically with a 50-60% overlap, completed by an outer layer of resin-impregnated glass fiber tape, wrapped helically with a small gap. Figure 2.8 shows the view of the cable insulated by wrapping 2 layers of Polyimide film.

In our study, we use 125µm thick Polyimide film (Upilex) manufactured by Ube Co. Ltd., Japan.

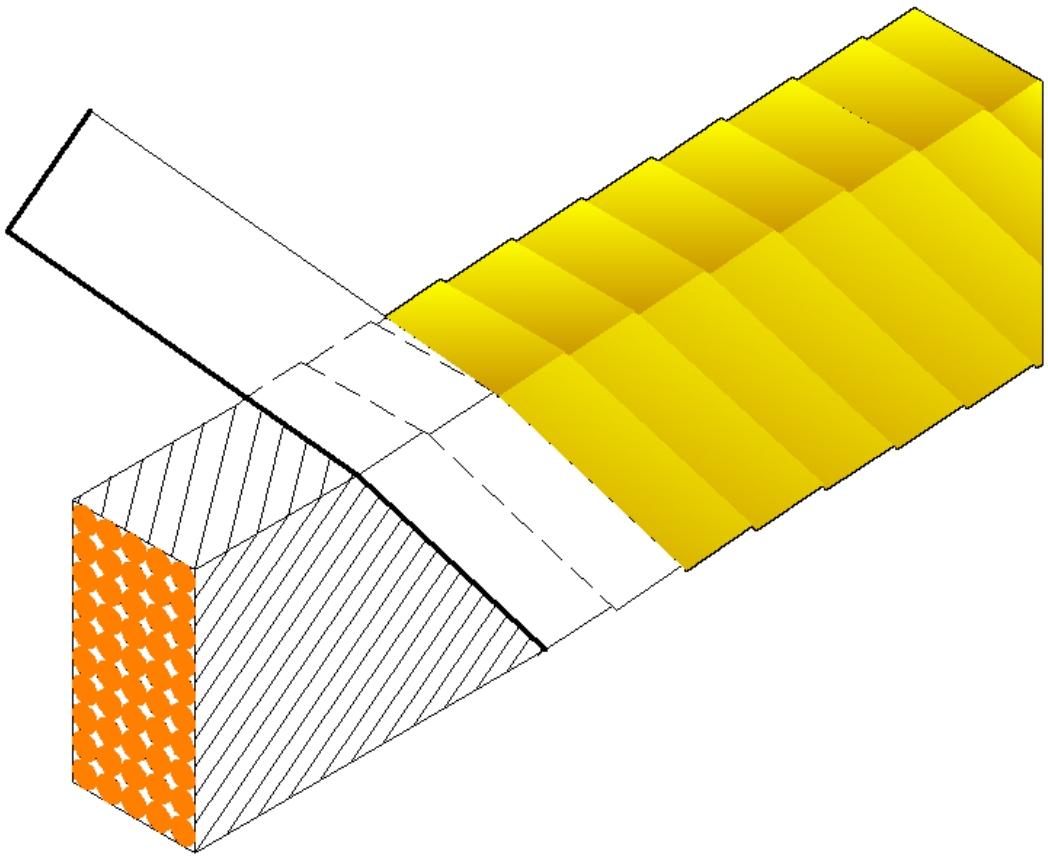

Figure 2.8: Superconducting cable being insulated using Polyimide film.

2.2.2 Dyneema Based Insulating Materials

Dyneema ® is a registered trademark in Japan. Polyethylene with an ultra high molecular weight is used as the starting material for the manufacturing of Dyneema fibers. Dyneema fibers are produced by gel spinning, a process invented and patented by the Du Point Company (DSM) in 1979. In the gel spinning process the molecules are dissolved in a solvent and spun through a spinneret [28]. In the solution the molecules that form clusters in the sold state become disentangled and remain in that state after the solution is cooled to give filaments. As the fiber is drawn, a very high level of macromolecular orientation is attained resulting in a fiber, as shown in fig. 2.9, with a very high tenacity and modulus. When formed to fibers, the polymer chains can attain a parallel orientation greater than 95% and a level of crystallinity of up to 85%. It has extremely long chains, with molecular weight numbering in the millions, usually between 2 and 6 million. Each chain is bonded to the others with so many Van der Waals bonds that the whole can support great tensile loads. The longer chain serves to transfer load more effectively to the polymer backbone by strengthening intermolecular interactions. This result in a very tough material, with the highest impact strength of any thermoplastic presently made. In normal polyethylene the molecules are not oriented and are easily torn apart.

Dyneema fiber expands to the longitudinal direction during cooling down from room temperature to liquid helium temperature, and fiber contracts to the transversal direction [29]. The coefficient of thermal expansion is –12E-06/K. Another unique property of Dyneema fiber is low coefficient of friction [30]. The molecular structure [31] of polyethylene fiber DYNEEMA® is

$$\left(-\underset{H}{\overset{H}{C}} - \underset{H}{\overset{H}{C}} - \right)_n$$

Typically, n is of the order of 10^6.

In our study, we used Dyneema cloth, Dyneema non-woven sheet and Dyneema random sheet as an insulating material. Toyobo Co. Ltd., Japan makes these materials. The properties of monofilament of Dyneema are given in table 2.4.

Dyneema fibers of all the samples are same. Therefore, the filament parameters of Dyneema based materials are same. The descriptions of these materials are discussed below.

Table 2.4: Properties of monofilament of Dyneema

Parameter	Value
Monofilament (dtex)	1.11
Density (g/cc)	0.97
Cross-sectional area (mm x mm)	1.14x10e-4
Young`s modulus (GPa)	88

where, 1dtex means 10,000 m of filament has 1 g of weight.

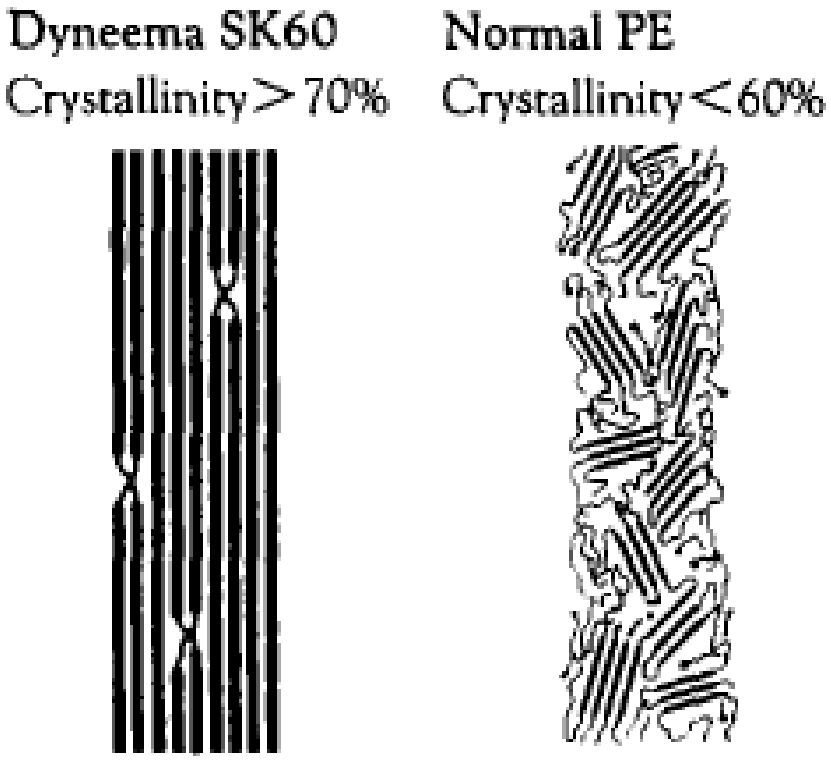

Figure 2.9: Molecular orientation in case of Dyneema SK60.

2.2.2.a Dyneema Cloth

In our study we used Dyneema SK-60. Used Dyneema cloth was a plain wave having 15 yarns/inch with 165 g/m^2. Figure 2.10 shows the Dyneema cloth sheet along with the sample holder and scissor used for cutting the cloth. The physical appearance of Dyneema cloth is bulky.

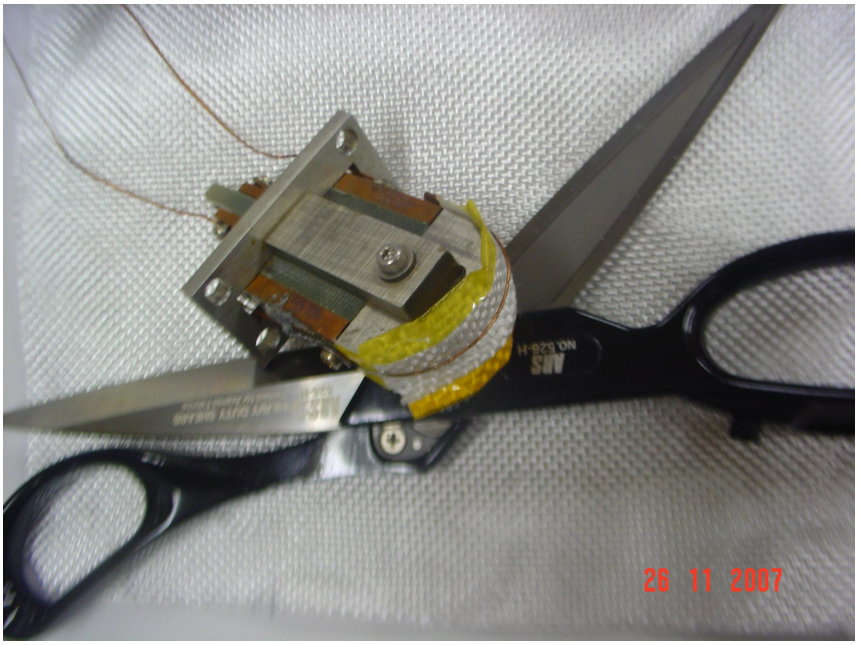

Figure 2.10: Sample holder along with Dyneema cloth sheet and scissor used for cutting.

2.2.2.b Dyneema Non-Woven Sheet

Dyneema non-woven sheet with 200 g/m^2 was used an insulating material. The length of Dyneema fiber is about 50mm. Figure 2.11 shows the photo of Dyneema non-woven sheet. The physical appearance of Dyneema non-woven cloth is like cotton sheet.

Figure 2.11: Photo of Dyneema non-woven sheet.

2.2.2.c Dyneema Random Sheet

Dyneema random sheet with 35 g/m^2 was used as an insulating material. The length of Dyneema fiber is about 38 mm. The volume fraction (%) is PE(DF)/PE/PP:50/25/25. Figure 2.12 shows the photo of Dyneema random sheet. The physical appearance of Dyneema random sheet is like a thin paper.

Figure 2.12: Photo of Dyneema random sheet.

2.2.3 Zylon Cloth

Zylon ® is a registered trademark in Japan. Zylon fiber is made from ploy-p-phenylenebenzobis-oxazole (PBO) by using a liquid crystalline spinning method and it has quite high strength and a rigid-rod chain molecular structure with high linearity [32]. It consists of rigid-rod chain molecules of poly (p-phenylene-2, 6-benzobisoxazole) (PBO). Zylon fiber expands to the longitudinal direction during cooling down from room temperature to liquid helium temperature, and fiber contracts to the transversal direction [33]. The coefficient of thermal expansion is -6E-06/K. Another unique property of Zylon fiber is low coefficient of friction [34]. In the course work of thesis, we have used Zylon-HM with 555 dTex. The property of monofilament of Zylon is given in table 2.5. Figure 2.13 shows the photo of Zylon cloth. The chemical structure of Zylon is shown below.

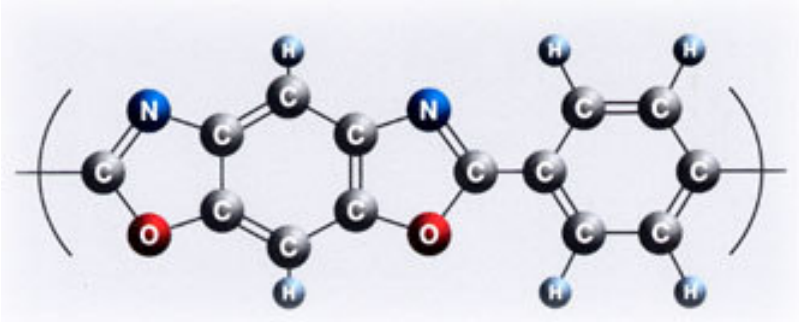

Chemical structure of Zylon.

Table 2.5: Properties of monofilament of Zylon

Parameter	Value
Monofilament (dtex)	1.7
Density (g/cc)	1.5
Cross-sectional area (mm x mm)	1.09x10e-4
Young`s modulus (GPa)	270

where, 1dtex means 10,000 m of filament has 1 g of weight.

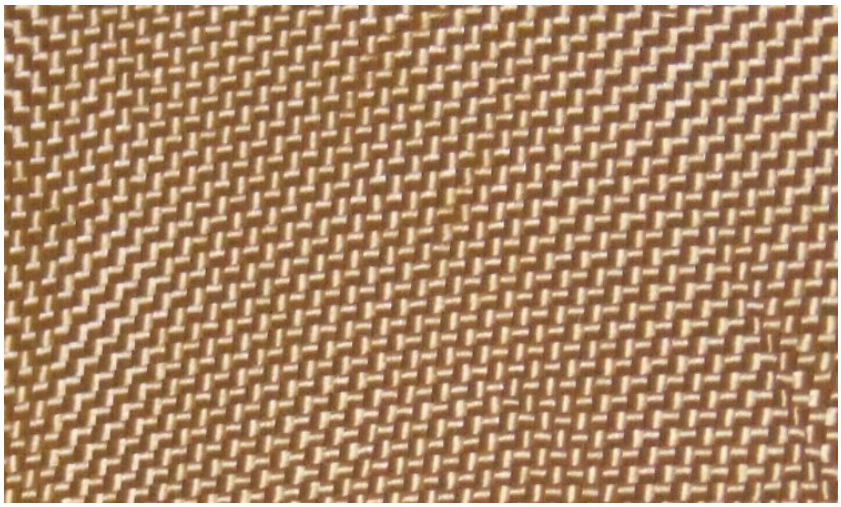

Figure 2.13: Photo of Zylon cloth.

2.2.4 Teflon

Teflon is the brand name for a number of fluorinated polymers. Teflon is polytetrafluroethylene (PTFE). It has excellent thermal and electrical insulation properties and a low coefficient of friction [35]. It also demonstrates good dimensional stability, reduced mold shrinkage, a smooth surface, and rigidity at high-use temperatures. Teflon is a polymer with repeating chains of –(CF2-CF2)- in it.

Chapter 3

Experiment methodology and findings

Experiments were conducted at 4.2 K to study the dependence of superconducting wire motion on the base insulating material under the influence of electromagnetic force. Voltage tap signal is measured using pen recorder or 16-bit data recorder with a sampling rate of 1MS/s. The experimental method implemented during the course work, experimental findings and comparison of measured data using pen recorder and data recorder are discussed in this chapter.

3.1 Experimental Procedure

3.1.1 Insulating Material

Measurements were carried out at 4.2 K using Polyimide film, Dyneema based materials, Zylon cloth and Teflon as an insulating material between the semi-circular head and the superconducting wire. The properties of these materials were discussed in chapter 2.

3.1.2 Cool Down

Superconducting solenoid magnet along with the sample holder is installed inside the 200 mm diameter vertical cryostat. During the cool down, tension of 28.4 N was applied to the superconducting wire. The main operation modes are:

Cool-down to 80 K;

Cool-down to 4.2 K;

Warm-up: After the final measurement, all the liquid helium from the cryostat is transferred back to gasbag and dumped into decanter until the liquid helium level meter show zero.

3.1.3 Current excitation scheme

The current in the superconducting wire was ramped from 0 A to 118 A. The current ramp up rate and ramp down rate was 0.84 A/s with a flat top time of 60 s. In order to examine the effect of the current ramp rate on the superconducting wire motion, ramp rate was changed from 0.4 A/s to 1.69 A/s. The typical current waveform is shown in fig. 3.1. The magnetic field of 6 T is kept constant during all the experiments.

Superconducting magnets shows a progressive improvement in performance after repeated quenching. This is termed as training effect. It is observed that superconductor moves to a stable position following successive repetition of current cycle. We performed the experiments to verify the phenomenon.

In case of superconductors, one cycle of field oscillation is sufficient to erase the history. Experiments were carried out by reversing the polarity of the current in the superconducting wire.

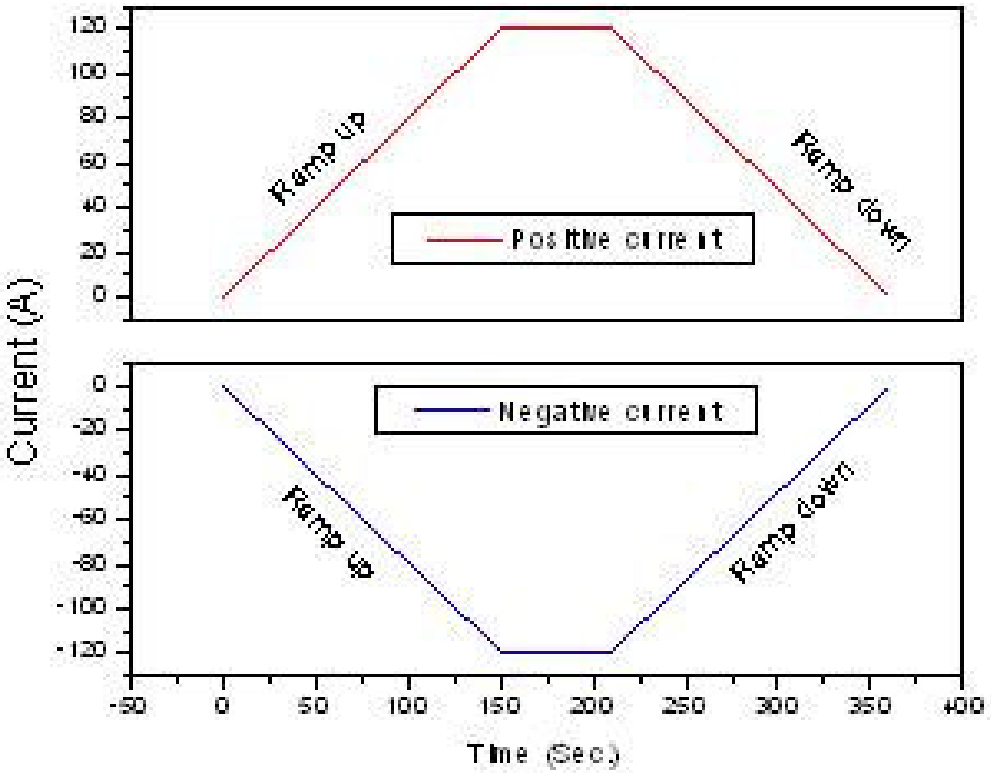

Figure 3.1: Current waveform pattern of superconducting wire.

3.1.4 Data Collection

Voltage taps to measure the signal due to the superconducting wire motion are connected at the end of the semi-circular head as shown in fig. 2.2. To reduce the voltage tap loop area, a groove was incorporated in the semi-circular head and the voltage tap wire (twisted pair of enameled copper wire 0.2 mm in diameter) was passed through it. In order to reduce noise, voltage tap wire is directly connected to the pen recorder [24] or a 16-bit data recorder with a sampling rate of 1 MS/s [25] to measure the voltage tap signal. Sudden wire motion was indicated by observing the voltage spike.

3.2 Experimental Findings

3.2.1 Experimental data obtained when voltage tap signal was fed to Pen recorder

3.2.1.1 Polyimide Film

Large amplitude wire motions were observed when tension was 7.1 N. The amount of frictional heat generated during these wire motions was sufficient to quench the wire. Figure 3.2 shows the voltage tap signal pattern measured using the pen recorder with the tension set at 14.1 N. Figure 3.3 shows the training behavior when the tension was 21.2 N. The number of voltage spikes reduced from ramp to ramp. At higher tension the voltage spike amplitude decreased.

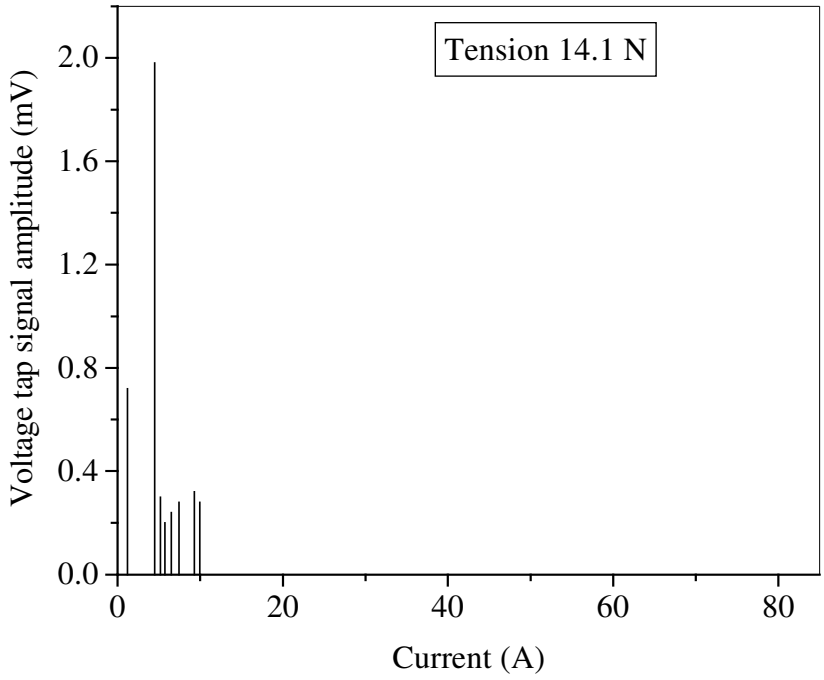

Figure 3.2: Voltage tap signal due to superconducting wire motion in case of Polyimide film.

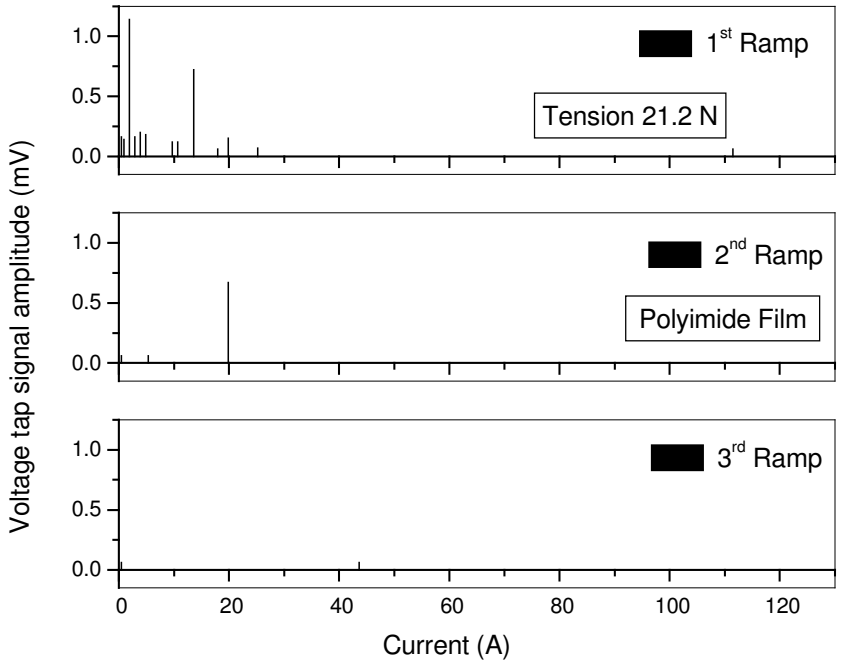

Figure 3.3: Training effect as observed in case of Polyimide film.

3.2.1.2 Dyneema Cloth

A large number of voltage spikes with low amplitude were observed when the tension was 7.1 N. Heat generated during these wire motions was not sufficient to quench the wire. The voltage tap signal pattern is shown in fig. 3.4. At low tension, the superconducting wire motion occurs during the current ramp up and current ramp down.

Reversing the polarity of current in the superconducting wire erases the history and no significant effect on the electromagnetic force need to start the superconducting wire motion was observed. However, an asymmetric voltage signal pattern was observed presumably due to asymmetric position of superconducting wire in the semi-circular head. A typical pattern obtained when the tension was 21.2 N is shown in fig. 3.5. At higher tension, the voltage spike amplitude decreased and relatively large electromagnetic force was needed to start the wire motion.

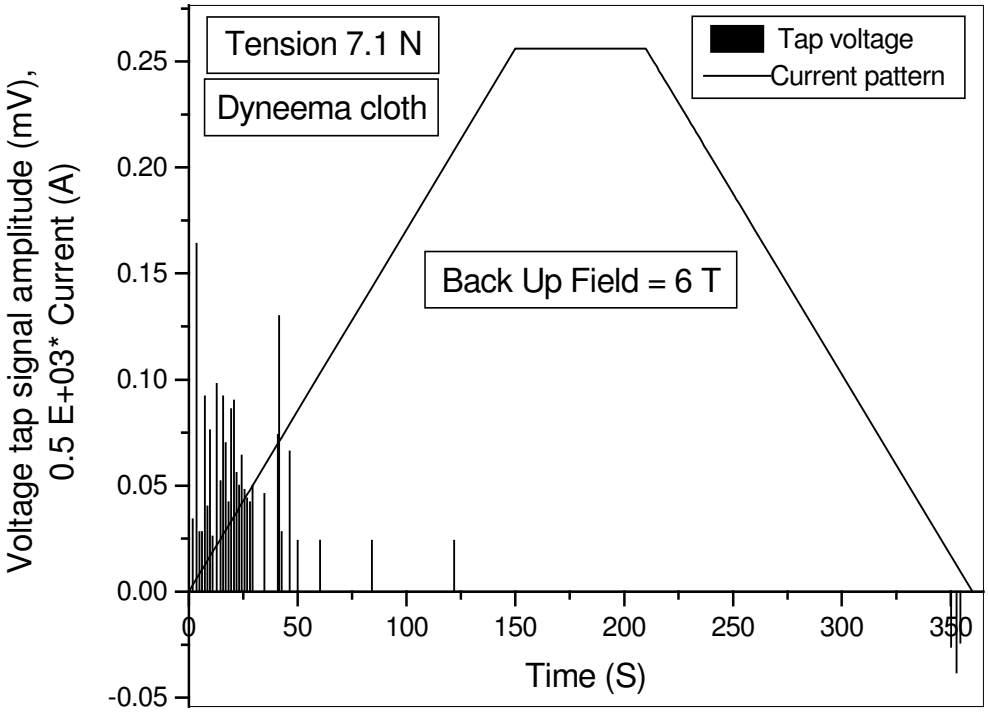

Figure 3.4: Typical current waveform and voltage tap signal due to wire motion in case of Dyneema cloth.

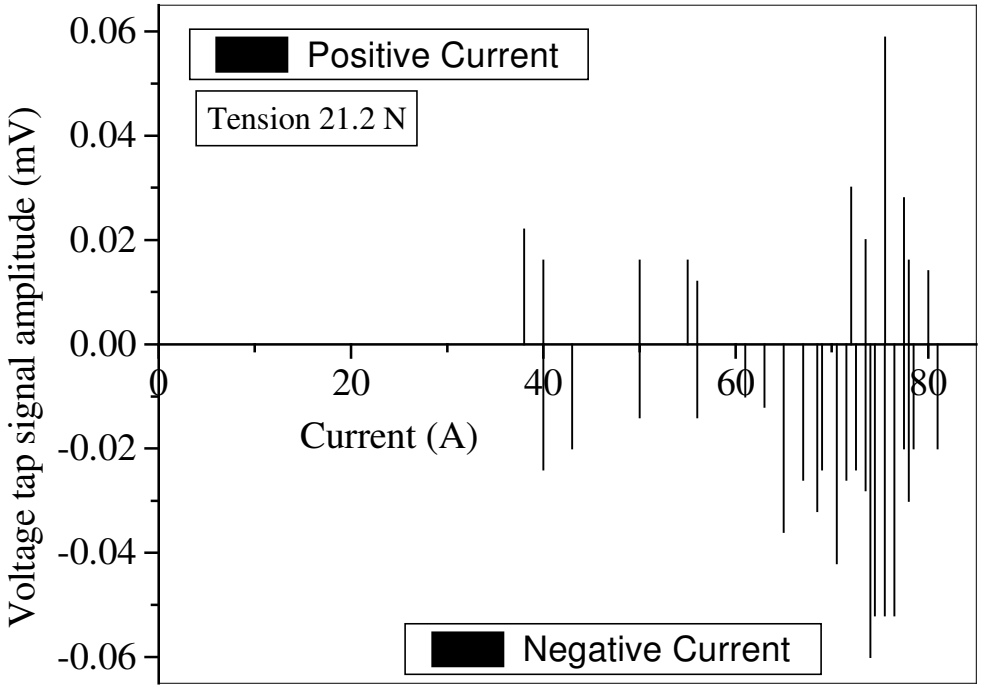

Figure 3.5: Typical voltage pattern due to wire motion after reversing the current polarity in case of Dyneema cloth.

3.2.1.3 Zylon Cloth

Superconducting wire motion occurs during the current ramp up and current ramp down when the tension was 7.1 N.

Figure 3.6 shows the voltage tap signal after reversing the current in the superconducting wire when the tension was 21.2 N.

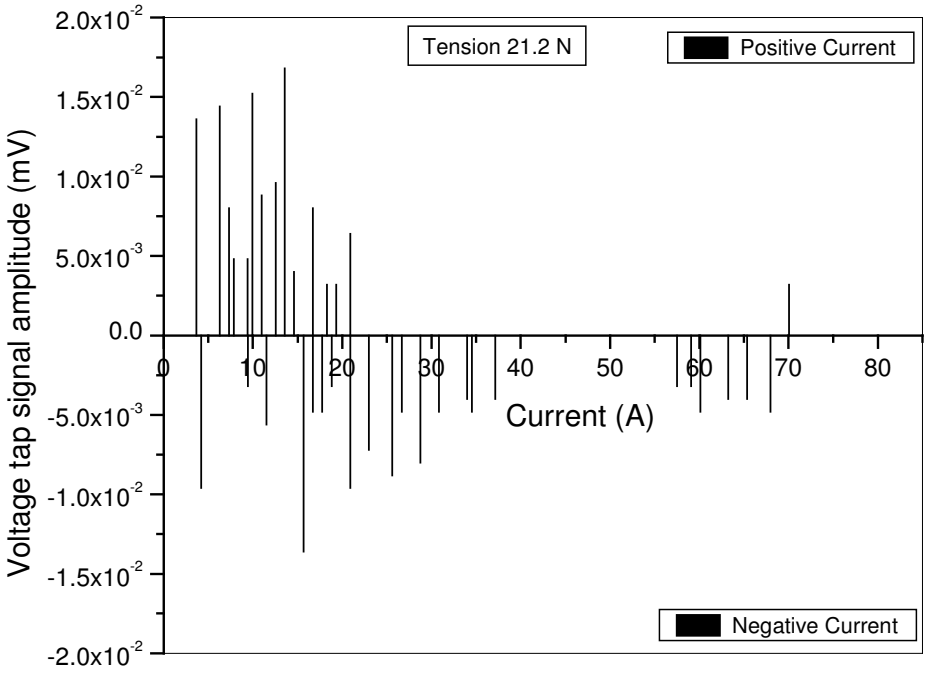

Figure 3.6: Typical voltage pattern due to wire motion after reversing the current polarity in case of Zylon cloth.

3.2.1.4 Dyneema Non-Woven Sheet

Figure 3.7 shows the voltage tap signal pattern after reversing the current polarity in the superconducting wire when the tension was 7.1 N.

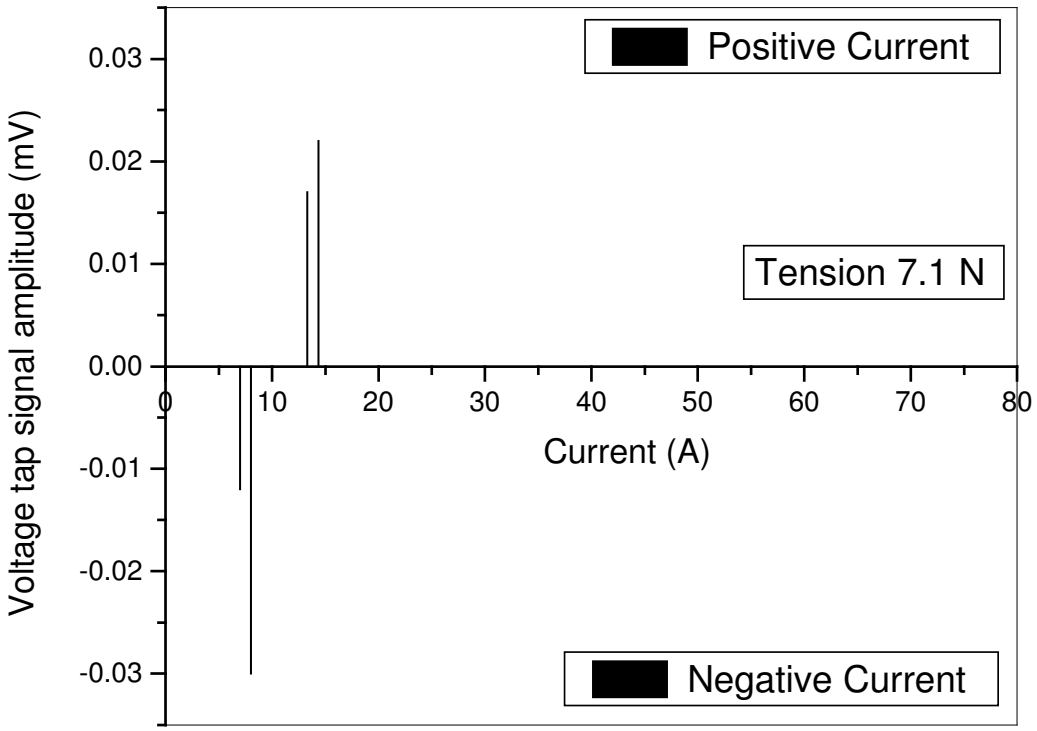

Figure 3.7: Typical voltage pattern due to wire motion after reversing the current polarity in case of Dyneema non-woven sheet.

3.2.1.5 Dyneema Random Sheet

Figure 3.8 shows the voltage tap signal when tension to the superconducting wire was 13.8 N. Figure 3.9 shows the dependence of voltage tap signal pattern on tension as a function of current.

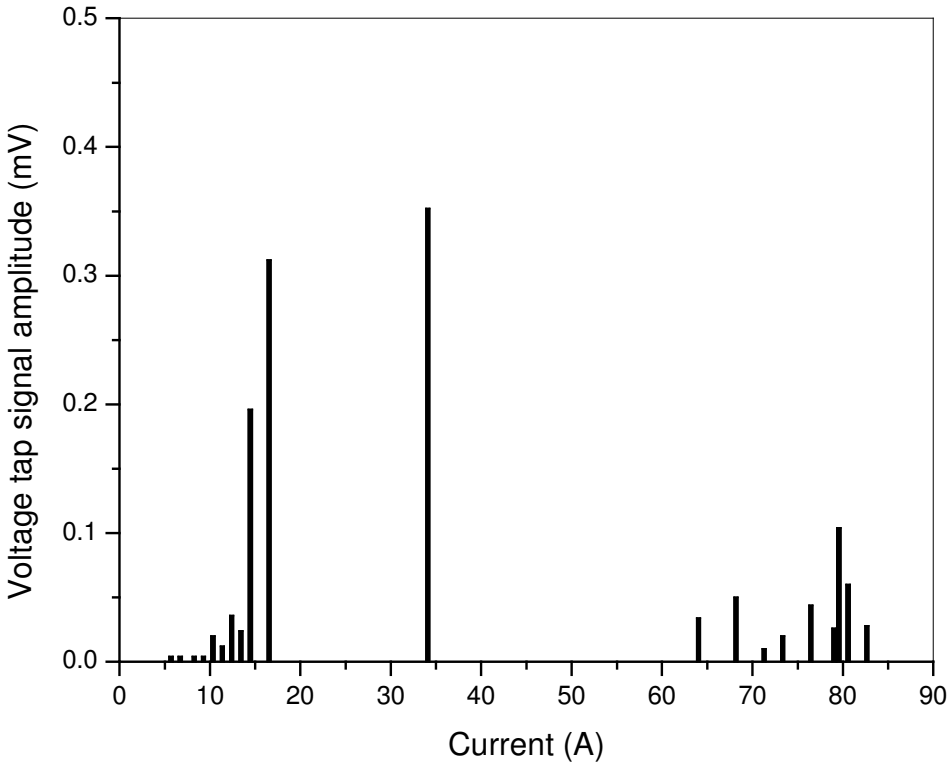

Figure 3.8: Typical voltage pattern due to wire motion after reversing the current polarity in case of Dyneema random sheet.

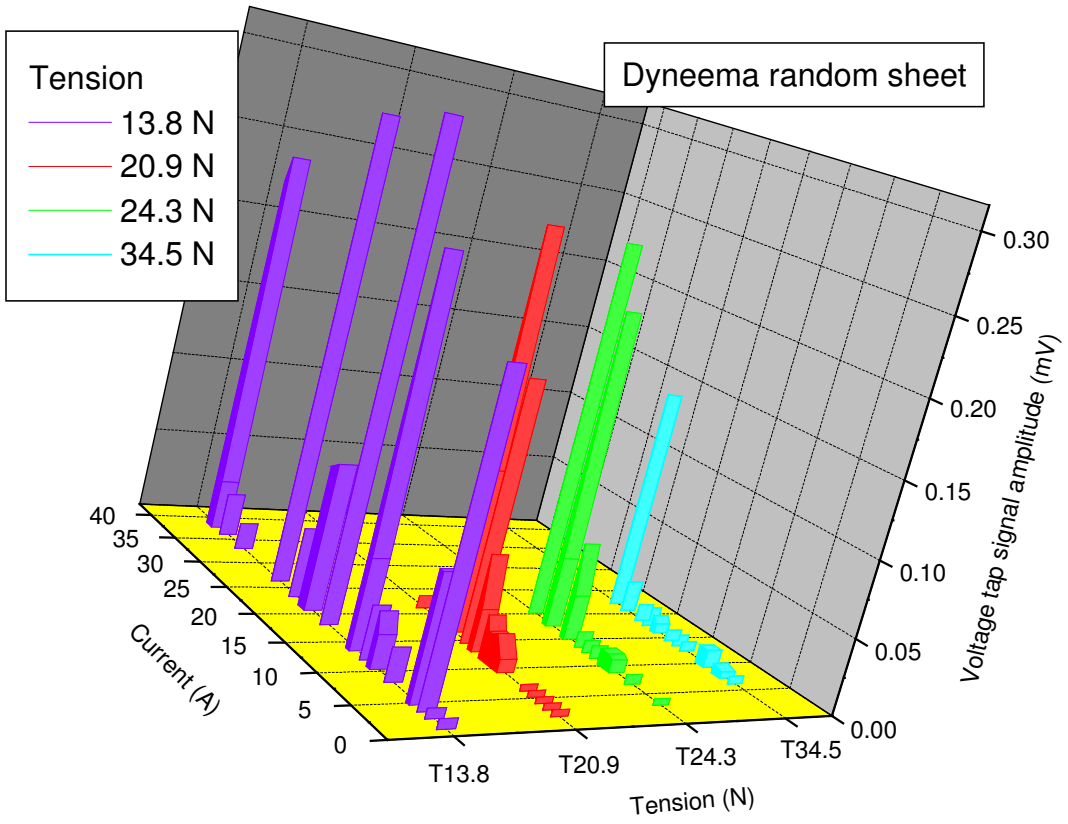

Figure 3.9: Voltage tap signal pattern as a function of tension and current in case of Dyneema random sheet.

3.2.1.6 Comparison of data measured using pen recorder

Figure 3.10 shows the comparison of voltage tap signal when Polyimide film, Dyneema based insulating materials and Zylon cloth are used as an insulating material between superconducting wire and semi-circular head. Many low amplitude voltage spikes were observed in case of Dyneema based insulating materials and Zylon cloth as compared to Polyimide film, which is attributed to low coefficient of friction. Tension to the superconducting wire was 21.2 N. Experiments were carried out under same experimental conditions.

Figure 3.11 shows the dependence of current at which superconducting wire motion starts as a function of tension. At larger tension, more electromagnetic force was needed to start the wire motion for all materials. One of the speculations for larger electromagnetic force in case of Dyneema cloth as compared to other insulating materials is the coarser texture of the cloth. The superconducting wire might have become embedded in the Dyneema cloth.

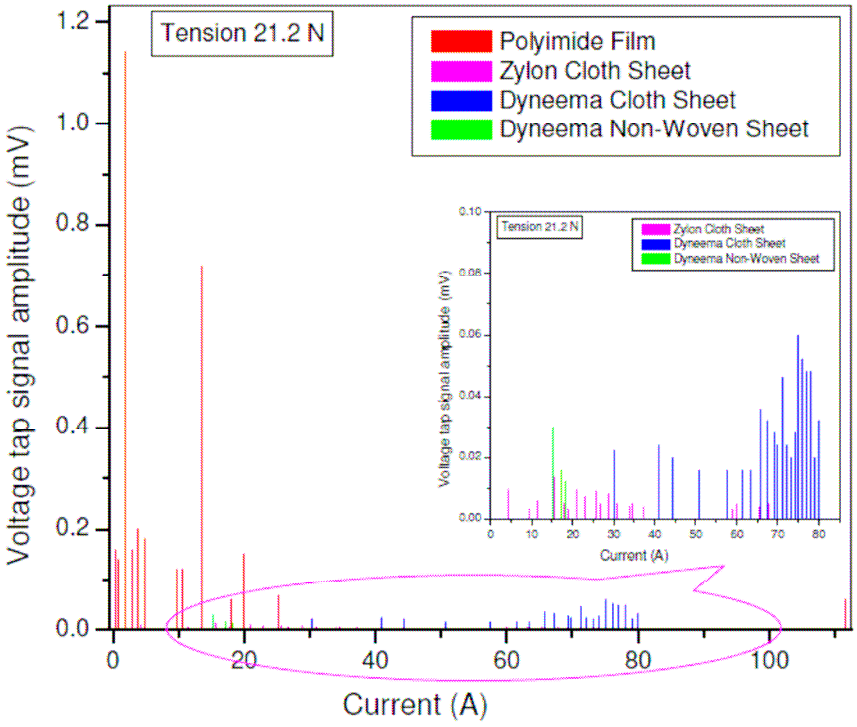

Figure 3.10: Comparison of voltage tap signal amplitude as a function of current.

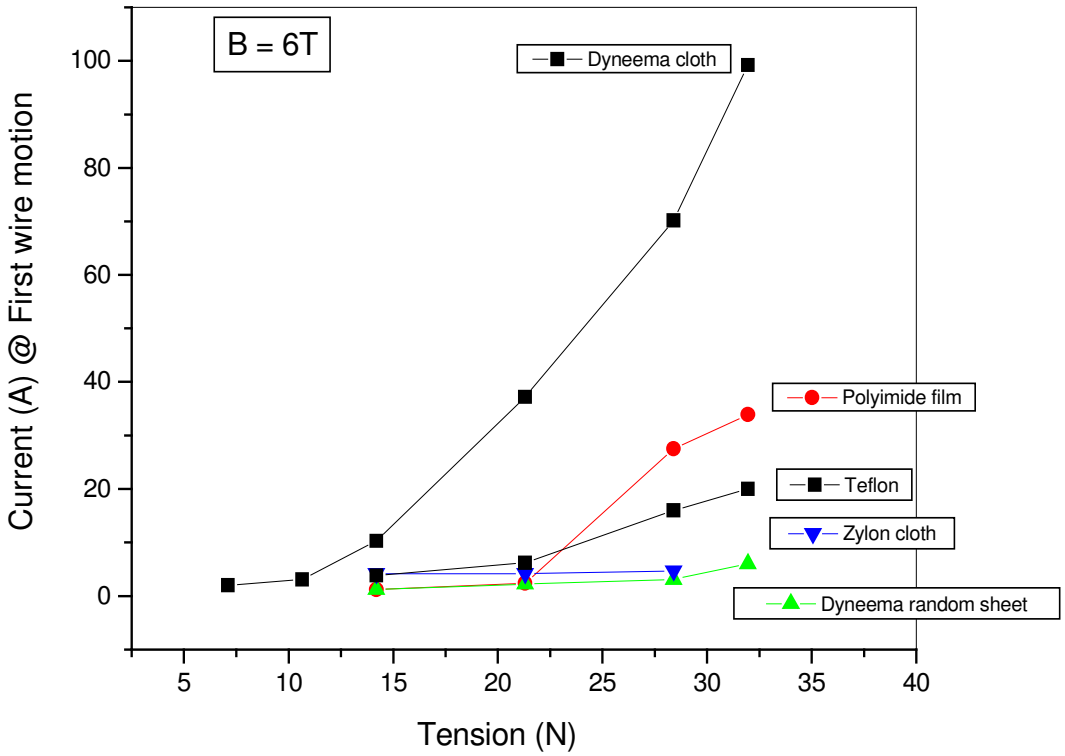

Figure 3.11: Dependence of wire motion on tension.

3.2.2 Experimental data obtained when voltage tap signal was fed to Data recorder

The pen recorder was not suitable for measurements of short duration pulses. So, we used a commercially available, 16-bit data recorder to measure the voltage tap signal. The sampling rate of the recorder was 1 MS/s. From the measured peak pattern, peak voltage tap signal amplitude, time duration of voltage spike, velocity of wire motion, distance moved by wire and energy dissipated due to wire motion is estimated (see appendix II for formulation).

3.2.2.1 Polyimide Film

Figure 3.12 shows the typical voltage tap signal when tension was 28.4 N. Figure 3.13 shows the peak voltage spike pattern. The FWHM is ~ 19 E-05 s. The amplitude of the peak voltage spike is 1.84 V. The current ramp rate was 0.84 A/s. The velocity of wire motion corresponding to peak voltage spike as estimated using Eq. (AII.5) is 15.46 m/s. The distance moved by wire as estimated using Eq. (AII.6) is 1.6 E-03 m. The energy dissipated as estimated using Eq. (AII.4) is 4.4 E-02 J. The velocity of wire motion and distance moved by wire falls in the macroscopic frictional disturbance category (stick-slip) [36].

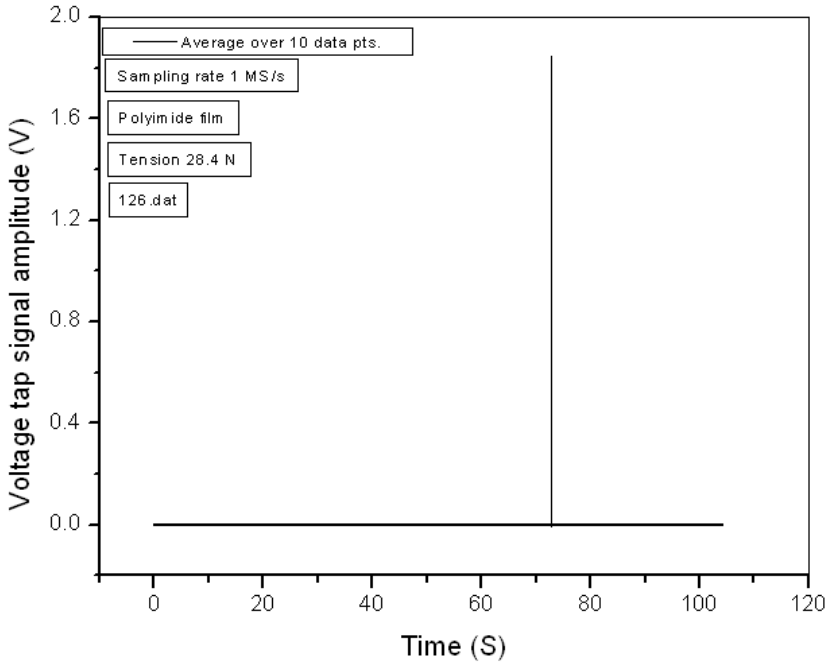

Figure 3.12: Typical voltage tap signal amplitude in case of Polyimide film.

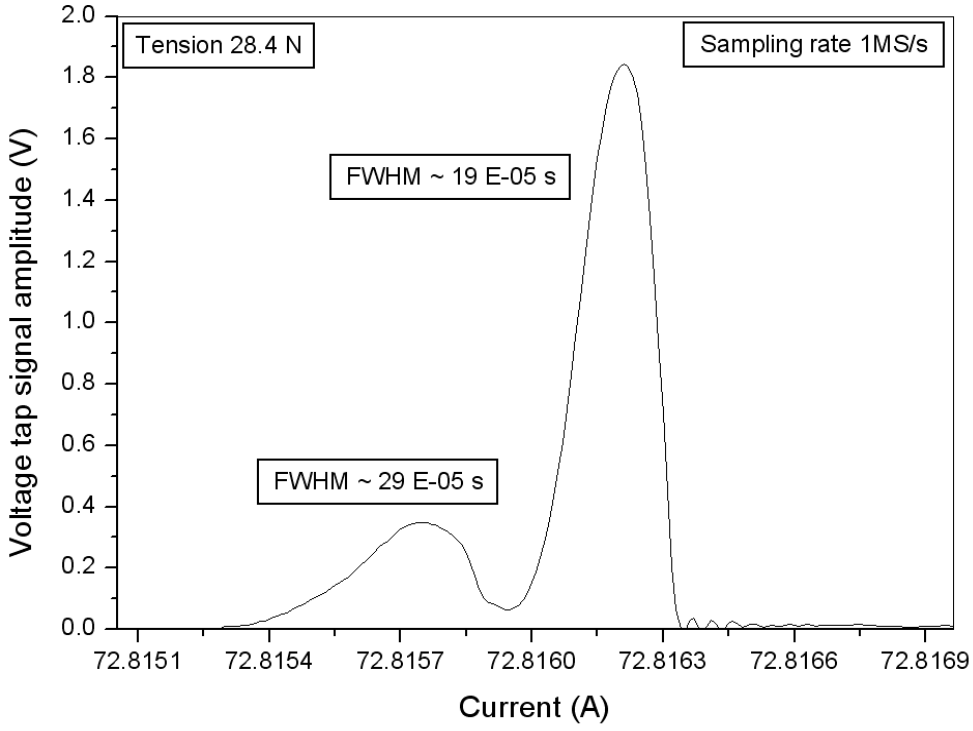

Figure 3.13: Peak voltage spike pattern in case of Polyimide film.

3.2.2.2 Dyneema Cloth

Figure 3.14 shows the typical voltage tap signal pattern when tension was 7.1 N. Figure 3.15 shows the peak voltage spike pattern. The FWHM is ~ 22 E-05s. The current ramp rate is 0.84 A/s. The amplitude of the peak voltage spike is 2.14 E-03 V. The velocity of wire motion corresponding to peak voltage spike as estimated using Eq. (AII.5) is 1.8 E-02 m/s. The distance moved by wire as estimated using Eq. (AII.6) is 2.4 E-06 m. The energy dissipated as estimated using Eq. (AII.4) is 5.5 E-05 J. The velocity of wire motion and distance moved by wire falls in the microslip frictional disturbance category [36].

Figure 3.16 shows the typical voltage tap signal amplitude as a function of averaging over various data points. Figure 3.17 shows the typical voltage spike amplitude / pattern dependence on averaging over data points. The voltage tap signal amplitude decreased and peak width increase with an increase in number of data points used for averaging. Figure 3.18 shows the voltage spike width as a function of current. The voltage spike width is of the same order for all the peaks. Figure 3.19 shows the product of voltage tap signal amplitude with voltage spike width as a function of current. Figure 3.20 shows the integrated voltage spike amplitude as a function of current. The total energy E (=ΣdE), released by the wire motion is shown in fig. 3.21, which is obtained by integrating the energy dissipated by wire motions.

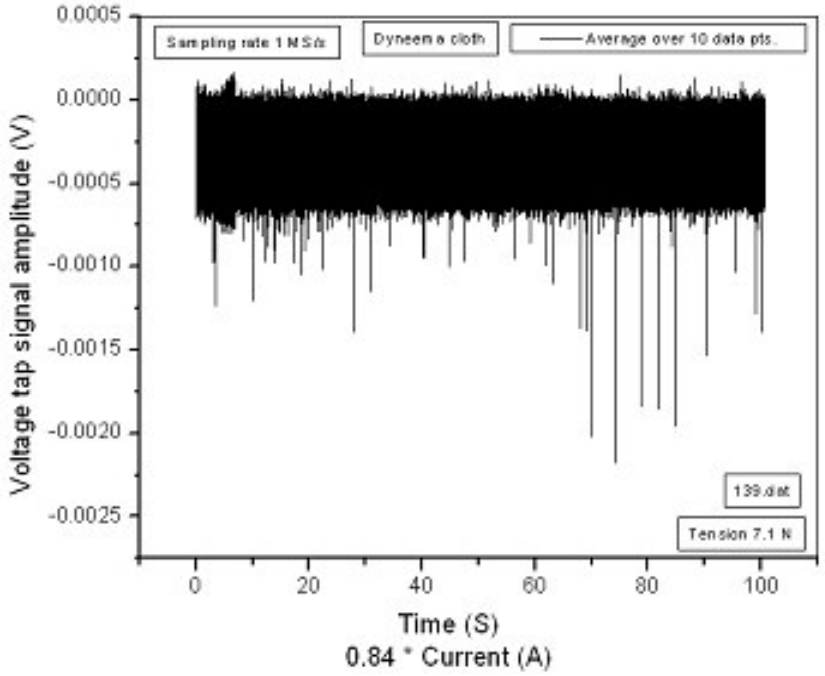

Figure 3.14: Typical voltage tap signal pattern in case of Dyneema cloth.

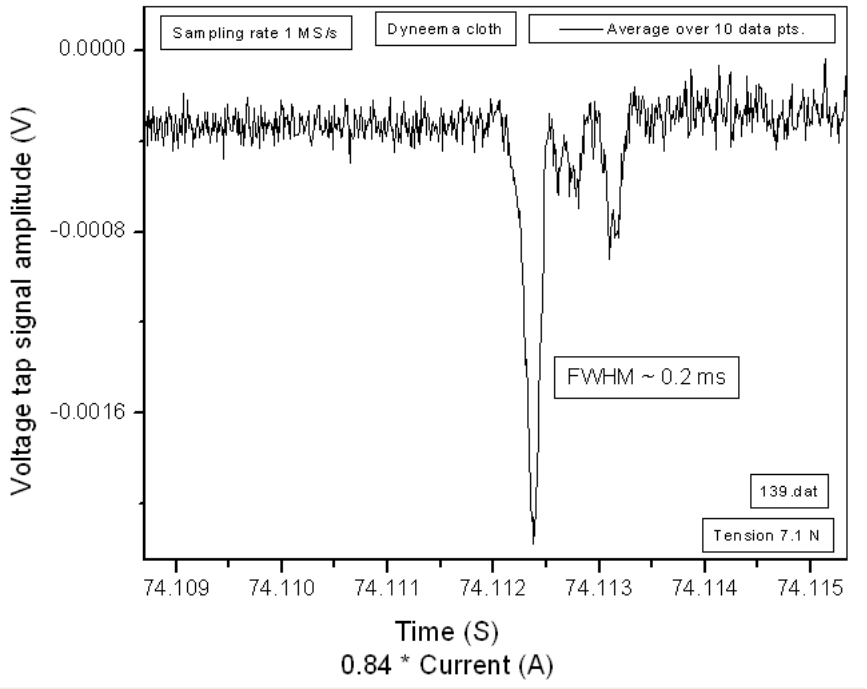

Figure 3.15: Peak voltage spike pattern in case of Dyneema cloth.

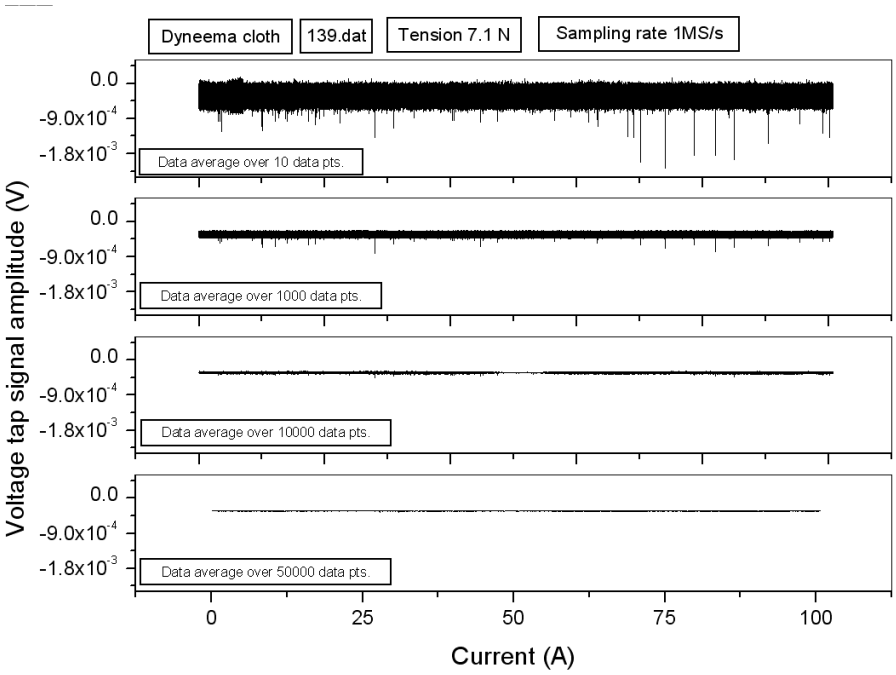

Figure 3.16: Typical voltage tap signal amplitude as a function of averaging of data points in case of Dyneema cloth.

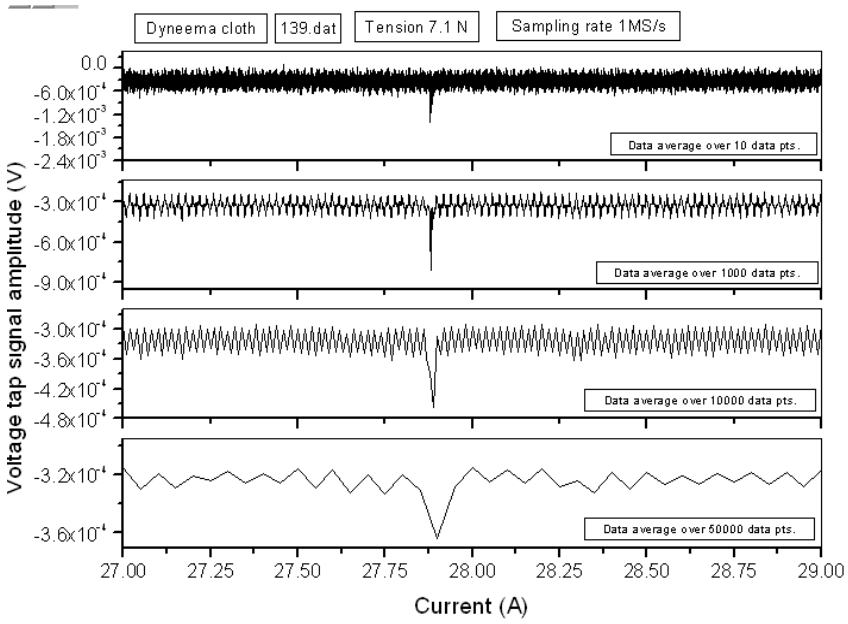

Figure 3.17: Typical voltage tap spike amplitude plot as a function of averaging of data points in case of Dyneema cloth.

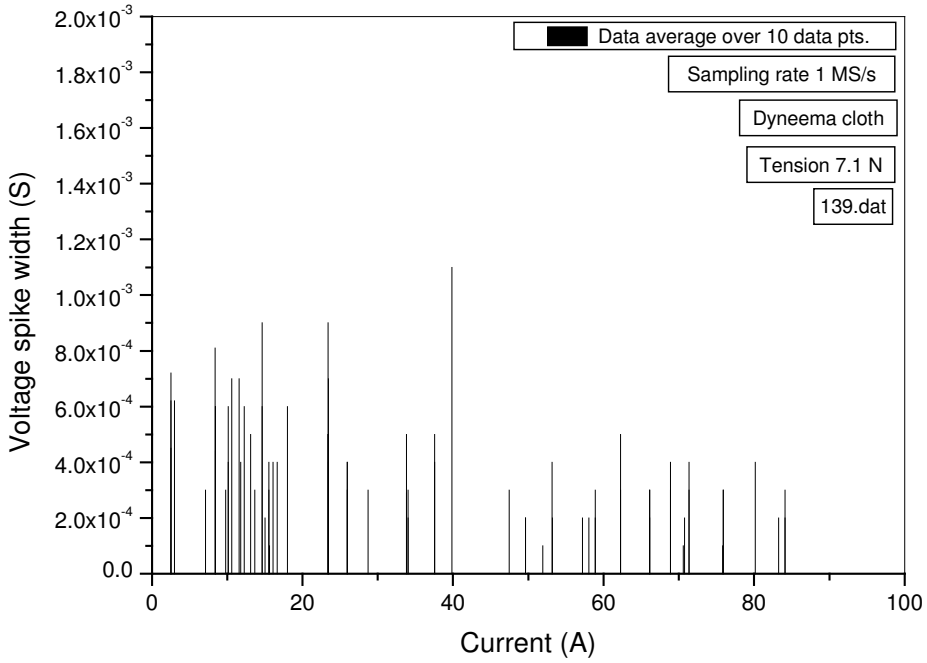

Figure 3.18: Voltage spike width as a function of current in case of Dyneema cloth.

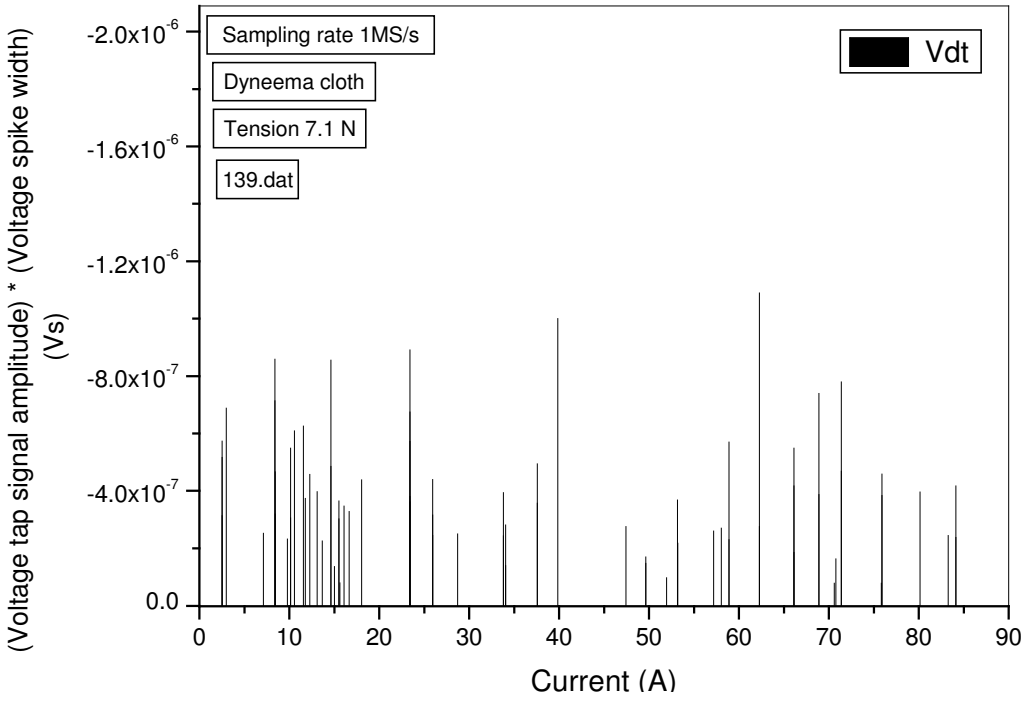

Figure 3.19: Product of voltage tap signal amplitude with voltage spike width as a function of current in case of Dyneema cloth.

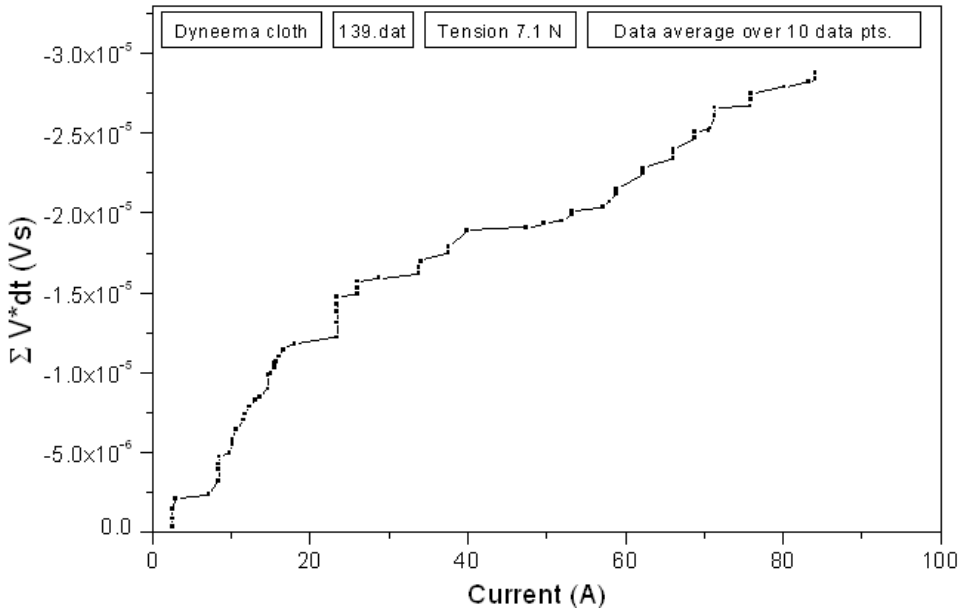

Figure 3.20: Integrated voltage spike amplitude as a function of current in case of Dyneema cloth.

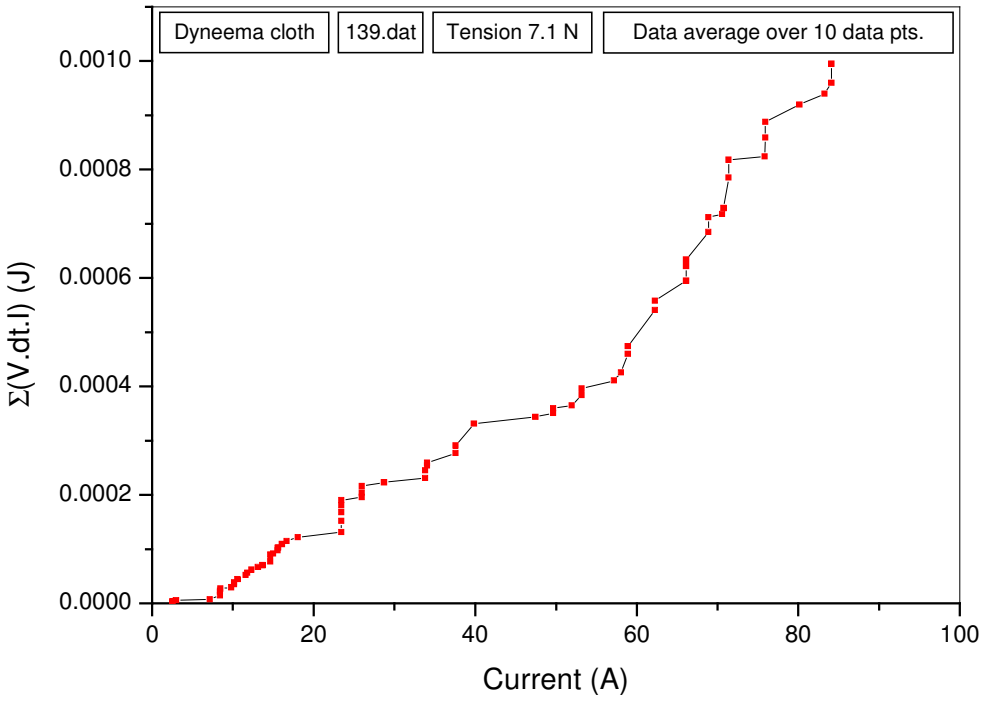

Figure 3.21: Total energy dissipated during wire motion as a function of current in case of Dyneema cloth.

3.2.2.3 **Dyneema Random Sheet**

Figure 3.22 shows the voltage tap signal pattern when tension is 15.1 N. Figure 3.23 shows the peak voltage spike pattern. The amplitude of the peak voltage spike is 3.59 E-03 V. The current ramp rate is 0.84 A/s. The maximum velocity of wire motion corresponding to peak voltage spike as estimated using Eq. (AII.5) is 3.0 E-02 m/s. The distance moved by wire as estimated using Eq. (AII.6) is 3.6 E-06 m. The energy dissipated as estimated using Eq. (AII.4) is 7.8 E-05J.

In order to observe the effect of current ramp on superconducting wire motion, measurements were carried out with a ramp rate of 1.69 A/s. Figure 3.24 shows the voltage tap signal pattern when tension was 15.1 N. Figure 3.25 shows the peak voltage spike pattern. The amplitude of the peak voltage is 3.66 E-03 V. From the peak profile, the FWHM was found to be ~1.5 E-04 s. The velocity of wire motion corresponding to the peak voltage spike as estimated using Eq. (AII.5) is 3.0 E-02 m/s. The distance moved by the wire as estimated using Eq. (AII.6) is 2.3 E-06 m. The energy dissipated as estimated using Eq. (AII.4) is 1.9 E-05 J.

No significant dependence of current ramp rate on voltage tap signal pattern, peak voltage spike amplitude, velocity of wire motion, distance moved by wire and energy dissipated was observed. The velocity of wire motion and distance moved by wire falls in the microslip frictional disturbance category [36].

Figure 3.26 shows the voltage tap signal plot when the measured data was averaged over 10 data points and 50,000 data points. A negative offset of magnitude ~ 3.0 E-04 V is observed. The value and direction of offset is independent of current ramp rate, tension to the superconducting wire and current direction in superconducting wire. The speculations are; the thermoelectric voltage of voltage tap signal wire and the voltage induced due to mutual inductance between voltage tap loop wire and superconducting wire.

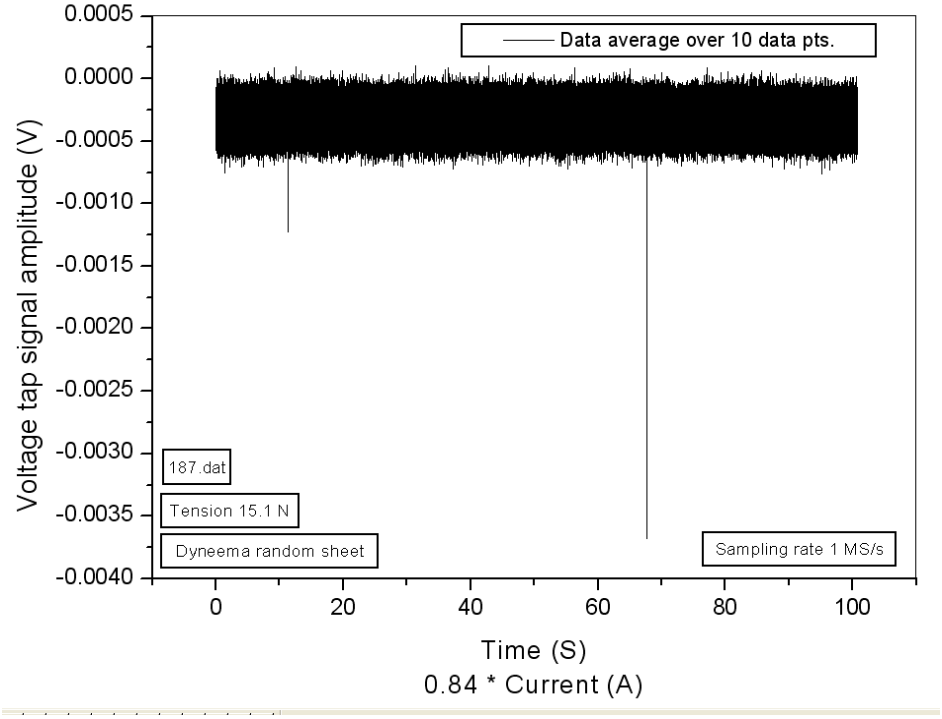

Figure 3.22: Typical voltage tap signal pattern in case of Dyneema random sheet when current ramp rate is 0.84 A/s.

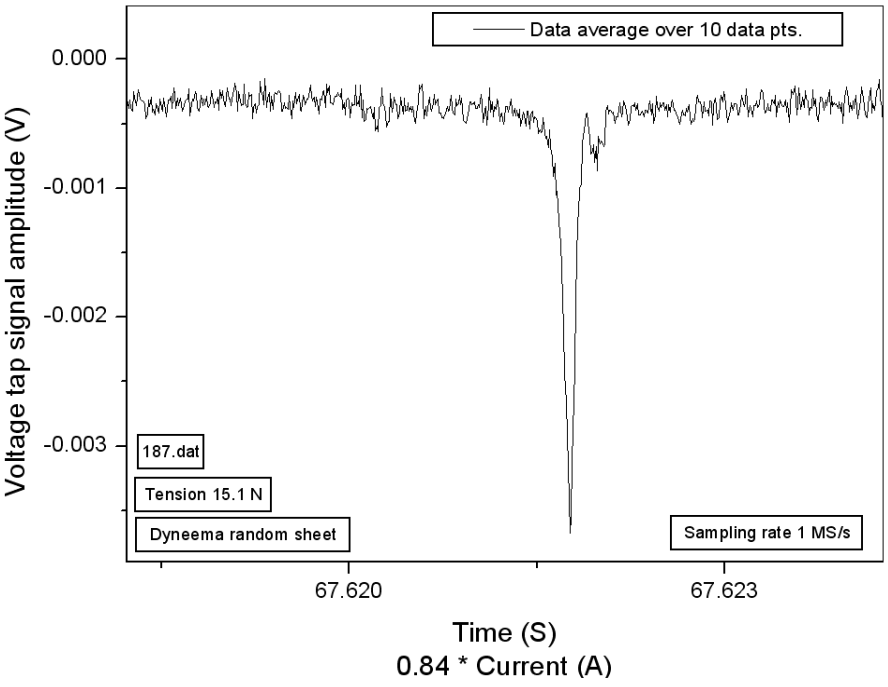

Figure 3.23: Peak voltage spike pattern in case of Dyneema random sheet when current ramp rate is 0.84 A/s.

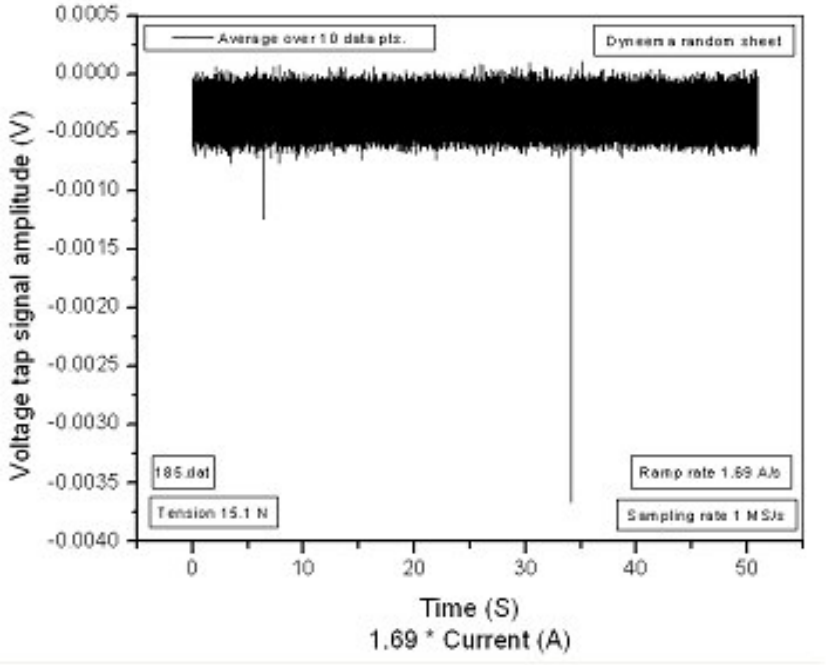

Figure 3.24: Typical voltage tap signal pattern in case of Dyneema random sheet when current ramp rate is 1.69 A/s.

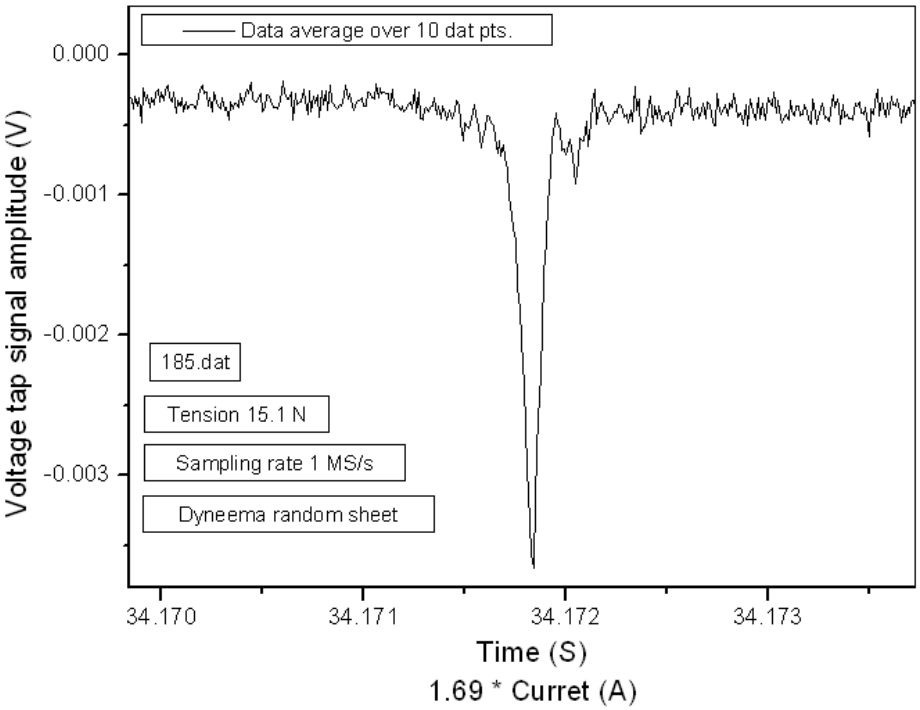

Figure 3.25: Peak voltage spike pattern in case of Dyneema random sheet when current ramp rate is 1.69 A/s.

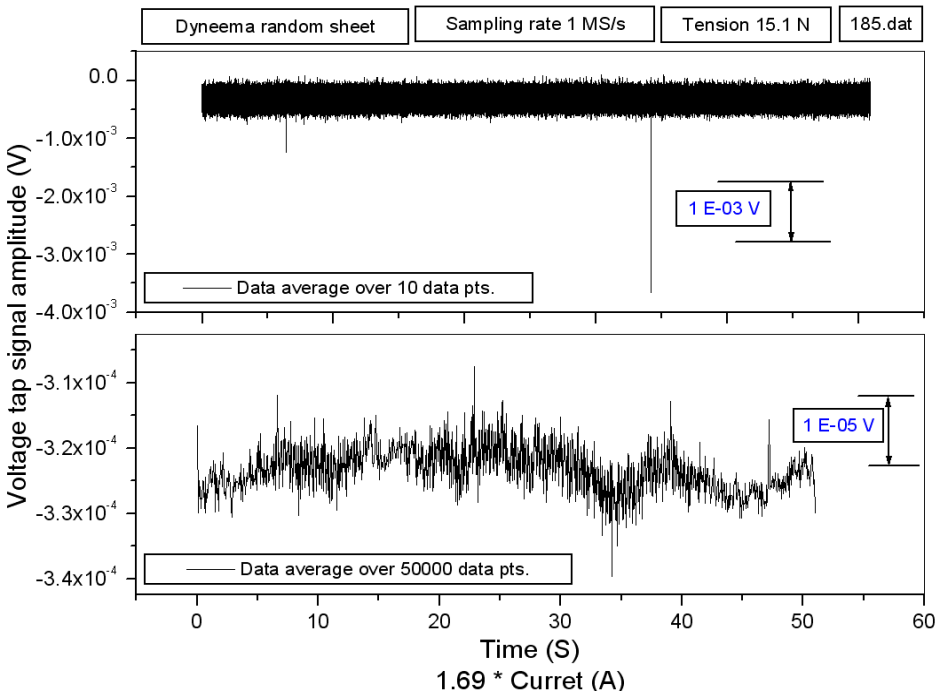

Figure 3.26: Typical voltage tap signal plot as a function of averaging of data points in case of Dyneema random sheet.

3.2.2.4 **Zylon Cloth**

Figure 3.27 shows the typical voltage tap signal pattern when tension was 28.4 N. Figure 3.28 shows the peak voltage spike pattern. The amplitude of the peak voltage spike is 7.37 E-03 V. The current ramp rate is 0.84 A/s. The velocity of wire motion corresponding to peak voltage spike as estimated using Eq. (AII.5) is 6.1 E-02 m/s. The distance moved by wire as estimated using Eq. (AII.6) is 5.2 E-06 m. The energy dissipated as estimated using Eq. (AII.4) is 2.5 E-04 J. The velocity of wire motion and distance moved by wire falls in the microslip frictional disturbance category [36].

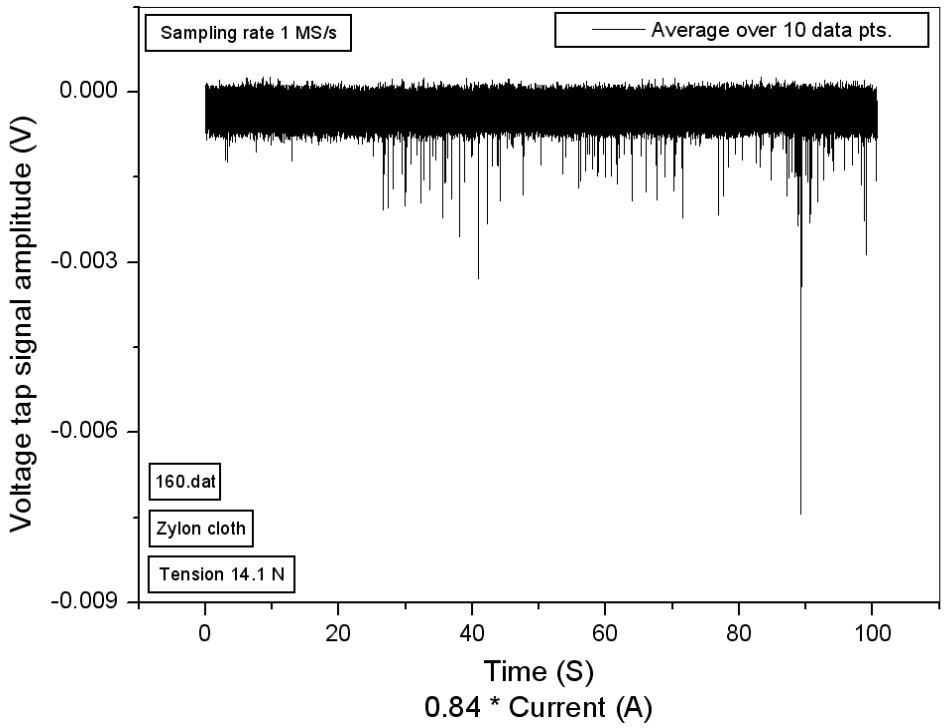

Figure 3.27: Typical voltage tap signal pattern in case of Zylon cloth.

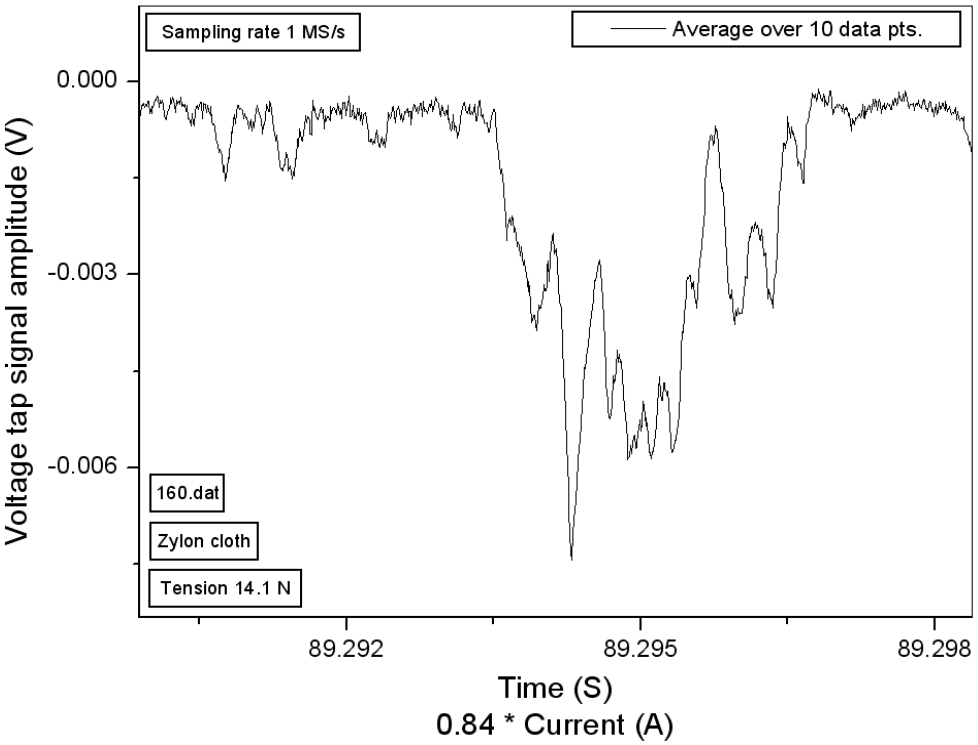

Figure 3.28: Peak voltage spike pattern in case of Zylon cloth.

3.2.2.5 **Teflon Sheet**

Figure 3.29 shows the typical voltage tap signal when tension was 15.1 N. Figure 3.30 shows the peak voltage spike pattern. The FWHM is ~ 48 E-05 s. The amplitude of peak voltage spike is 14.44 E-03 V. The current ramp rate is 1.69 A/s. The sampling rate of the recorder was 1MS/s. The velocity of wire motion corresponding to peak voltage spike as estimated using Eq. (AII.5) is 1.2 E-01 m/s. The distance moved by wire as estimated using Eq. (AII.6) is 4.7 E-05 m. The energy dissipated as estimated using Eq. (AII.4) is 3.5 E-04 J.

Figure 3.31 shows the peak voltage spike pattern when the tension was 35.8 N. The FWHM is ~23 E-05 s. It is evident that FWHM is independent of the tension. The velocity of wire motion and distance moved by wire falls in the microslip frictional disturbance category [36].

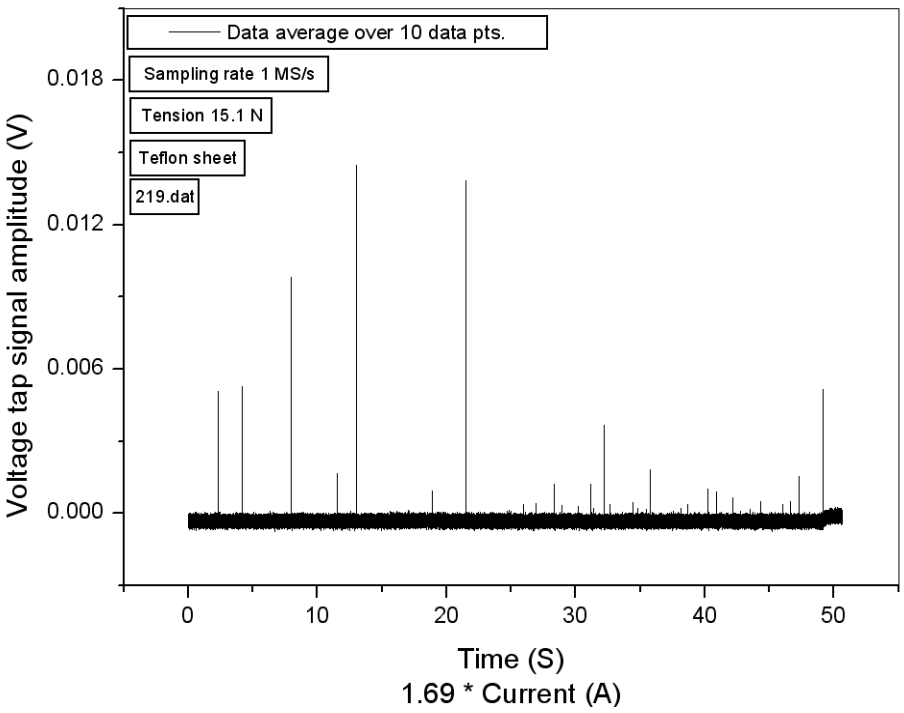

Figure 3.29: Typical voltage tap signal pattern in case of Teflon sheet.

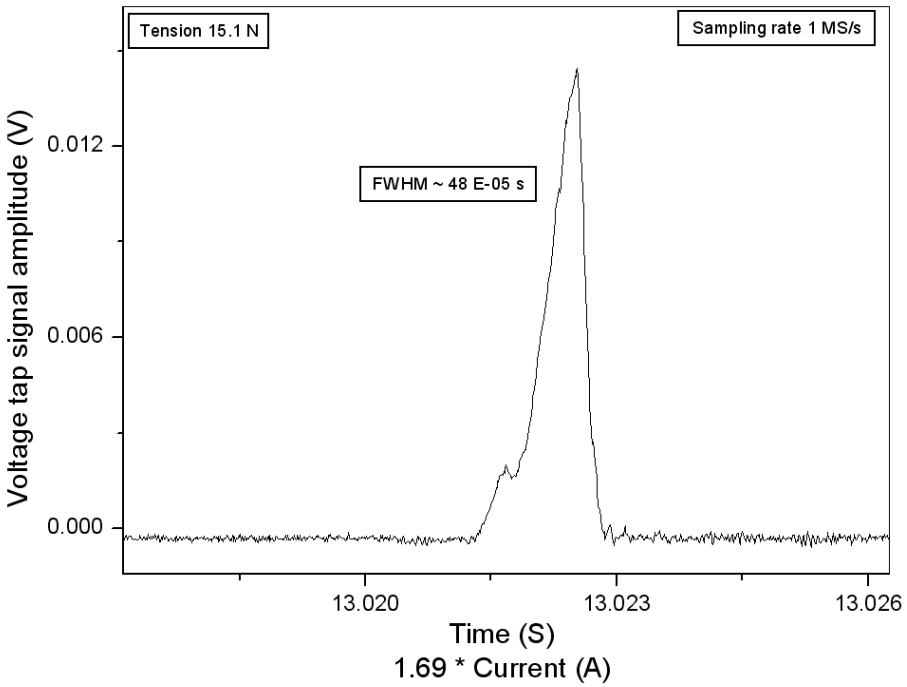

Figure 3.30: Peak voltage spike pattern in case of Teflon sheet when tension is 15.1 N.

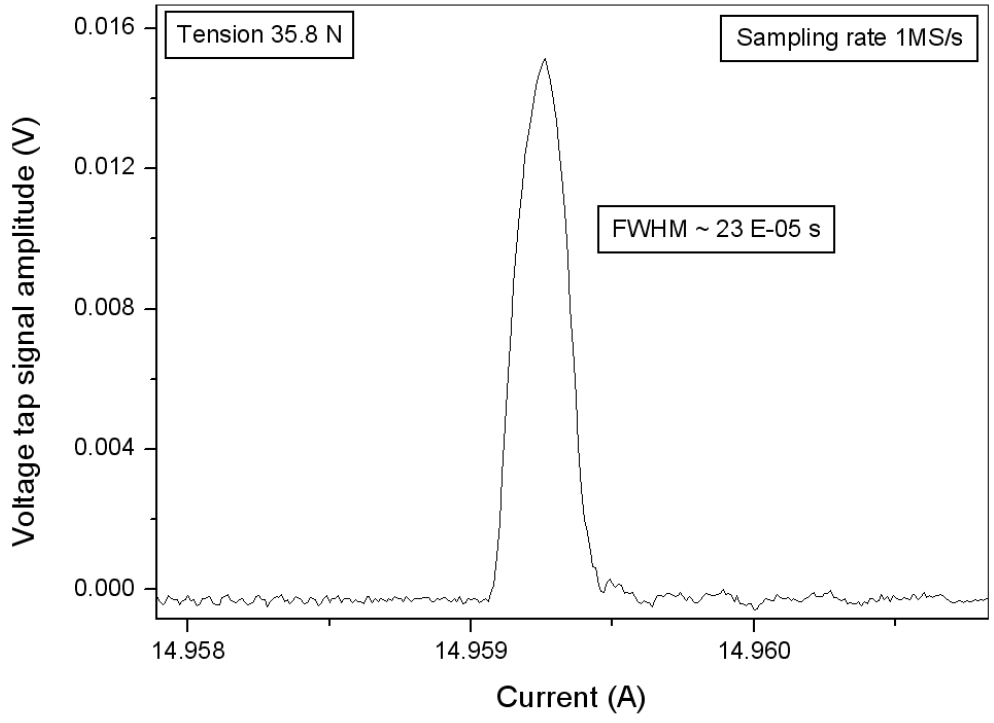

Figure 3.31: Peak voltage spike pattern in case of Teflon sheet when tension is 35.8 N.

3.2.2.6 Comparison of data measured using data recorder:

Figure 3.32 shows the comparison of voltage tap signal amplitude as a function of current for various samples. Low amplitude voltage spikes in case of Zylon / Dyneema based materials as compared to Polyimide film is attributed to low coefficient of friction. Similar voltage signal pattern (a large number of small amplitude voltage spikes) in case of Dyneema cloth and Zylon cloth is attributed to similar texture of material. Both the materials have no other materials in them i.e., they consists of monofilament of Dyneema / Zylon. Hence, smooth wire motion occurs because of low coefficient of friction of Dyneema / Zylon monofilaments.

The voltage signal pattern in case of Dyneema random sheet is similar to Teflon sheet, which is attributed to short length of Dyneema fiber and presence of polypropylene (PP) and polyethylene (PE) in Dyneema random sheet.

Figure 3.33 shows the peak voltage tap signal amplitude, time duration of voltage spike, velocity of wire motion, distance moved by wire and energy dissipated during peak voltage spike for various insulating materials used during the course work. The peak voltage tap signal amplitude, velocity of wire motion, distance moved by wire and energy dissipated during peak voltage spike in case of Polyimide film is more than 2 order of magnitude larger than Dyneema based insulating materials and Zylon cloth. The time duration of voltage spike is found to be same order for all the samples.

The velocity of wire motion and distance moved by wire falls in the macroslip frictional disturbance category in case of Polyimide film whereas in case of Zylon / Teflon / Dyneema based materials it falls in the microslip frictional disturbance category [36].

Table 3.1 shows the comparison of peak voltage tap signal amplitude, time duration of voltage spike, velocity of wire motion, distance moved by wire, kinetic energy and energy dissipated during peak voltage spike for various materials used in the study.

A negative offset was observed during the measurements. The value and direction of offset is independent of current ramp rate, current direction in superconducting wire and sample characteristics. Measured data average over 10 data

points and 50, 000 data points are shown in fig. 3.26. The magnitude of offset voltage is ~ 3.0 E-04 V. The speculations are; the thermoelectric voltage of voltage tap signal wire and the voltage induced due to mutual inductance between voltage tap loop wire and superconducting wire.

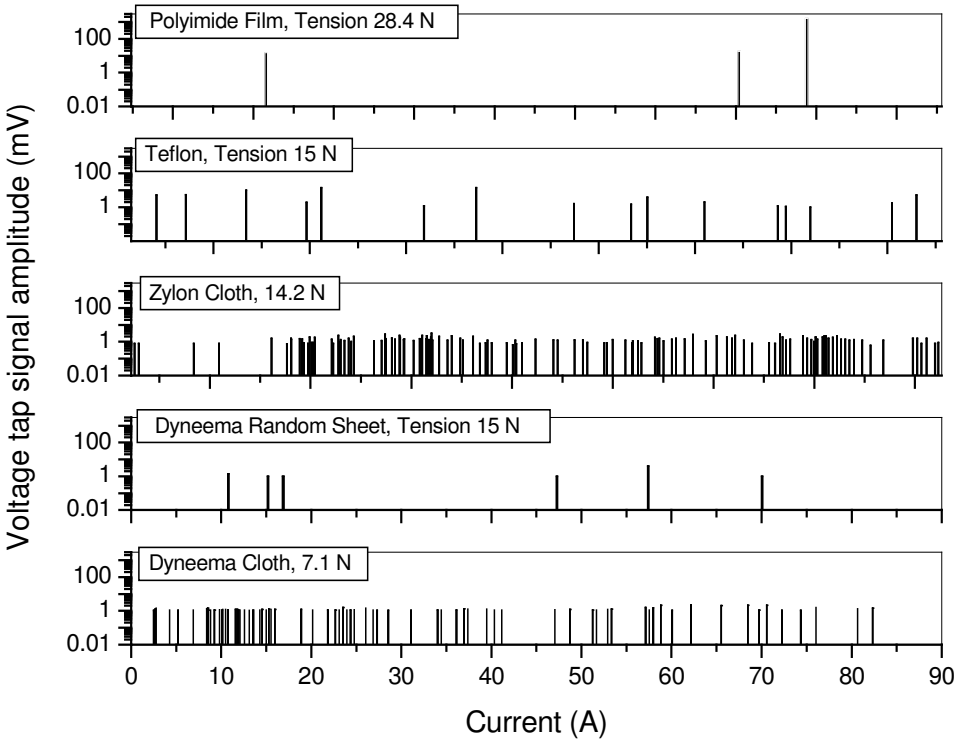

Figure 3.32: Comparison of voltage tap signal amplitude as a function of current for various samples.

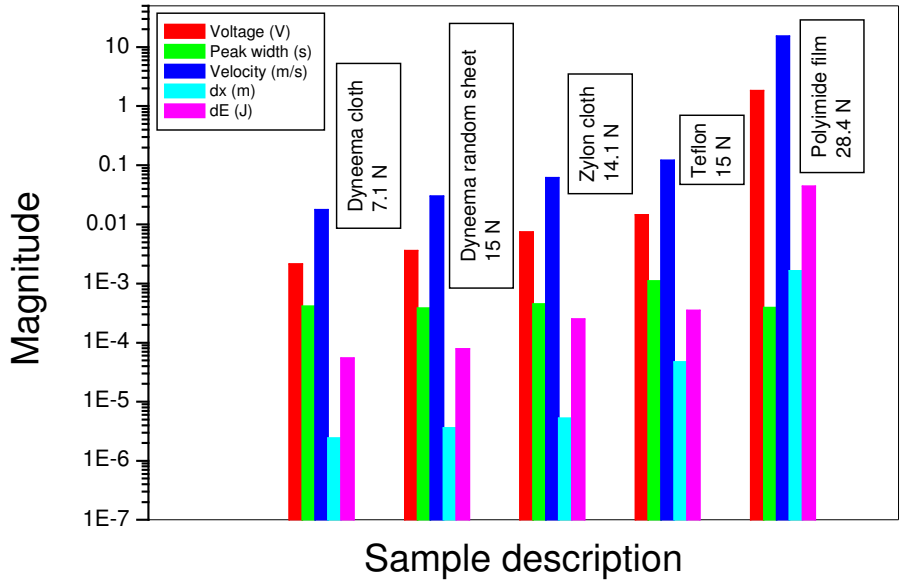

Figure 3.33: Comparison of voltage tap signal amplitude, peak voltage spike width and energy dissipated for various samples.

Table 3.1: Comparison of peak voltage tap signal amplitude, velocity of wire motion and energy dissipated due to wire motion for various materials.

Sample⇨	Dyneema cloth	Dyneema random sheet	Zylon cloth	Teflon	Polyimide film
File Name ⇨ Parameter⇩	139.dat	187.dat	160.dat	219.dat	126.dat
Tension	7.1 N	15 N	14.1 N	15 N	28.4 N
Peak voltage (V)	0.00214	0.003598	0.00737	0.01444	1.8434
Time to reach max. voltage (s)	2.7 E-04	2.4 E-04	1.7 E-04	7.8 E-04	2.14 E-04
Total pulse duration (s)	4.1 E-04	3.8 E-04	4.5 E-04	1.1 E-03	3.9 e-04
Velocity (m/s)	1.783E-02	2.998E-02	6.142E-02	1.203E-01	1.536E+01
Acceleration (m/s^2)	6.605E+01	1.249E+02	3.613E+02	1.543E+02	7.178E+04
dx (m)	2.408E-06	3.598E-06	5.220E-06	4.693E-05	1.644E-03
Ke (J)	1.034E-08	2.922E-08	1.226E-07	4.706E-07	7.669E-03
dE (J)	5.457E-05	7.766E-05	2.487E-04	3.494E-04	4.400E-02

3.2.3 Comparison between pen recorder and data recorder data

The voltage tap signal was measured using pen recorder and 16-bit data recorder. The voltage tap signal amplitude measured by the data recorder was more than 1 order of magnitude greater than with the pen recorder. The difference in the voltage tap signal amplitude was validated by feeding a short duration pulse generated using a pulse generator to the data recorder and the pen recorder. Figure 3.37 shows the measured pulse pattern using data recorder and pen recorder when a pulse of 12 ms and 1 V was feed using pulse generator.

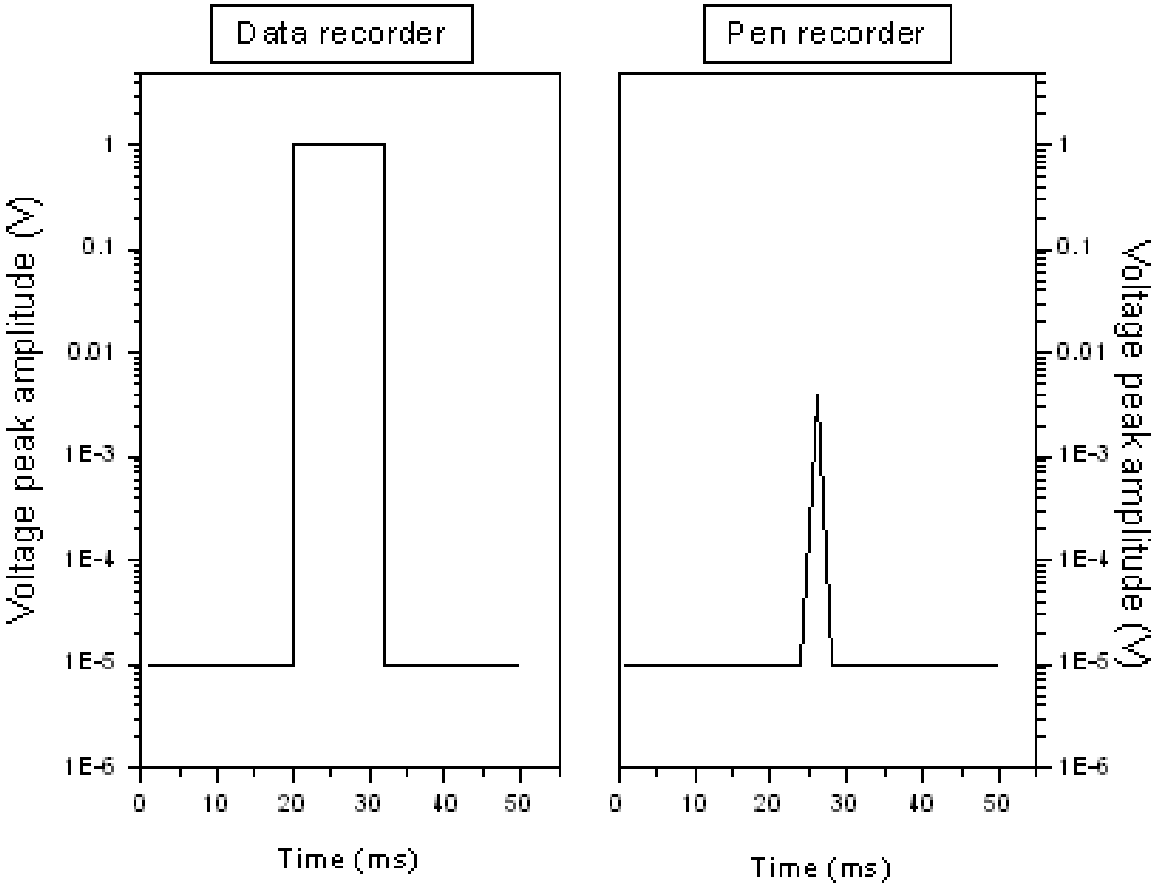

Figure 3.34: Voltage pulse pattern measured using data recorder and pen recorder.

Chapter 4

Conclusion

To study the superconducting wire motion under the influence of electromagnetic force, we developed an experimental setup and verified the effectiveness of this system. The main objective of our study is to examine the time dependence profile of superconducting wire motion in magnetic field on frictional property of insulating materials, tension on the superconducting wire, current ramp rate and effect of polarity of current in the superconducting wire.

Large amplitude wire motions were observed when the insulating material was Polyimide film and tension was 7.1 N. The amount of frictional heat generated during these wire motions was sufficient to quench the wire.

A large number of voltage spikes with low amplitude were observed when the insulating material was Dyneema / Zylon cloth and tension was 7.1 N. Heat generated during these wire motions was not sufficient to quench the wire. At low tension, the superconducting wire motion occurs during the current ramp up and current ramp down.

At higher tension the voltage spike amplitude decreased and relatively large electromagnetic force was needed to start the wire motion. One of the speculations for larger electromagnetic force in the case of Dyneema cloth as compared to other insulating materials used during study is the coarser texture of the cloth. The superconducting wire might have become embedded in the Dyneema cloth. To overcome the embedding of the superconducting wire in the Dyneema cloth, sheet material was fabricated with Dyneema fiber.

The peak voltage tap signal amplitude, velocity of wire motion, distance moved by wire and energy dissipated due to wire motion in case of Polyimide film is more than an 2 order of magnitude larger than Zylon / Dyneema based insulating materials. Low voltage tap signal amplitude in case of Zylon / Dyneema based materials as compared to Polyimide film is attributed to low coefficient of friction.

Hence, use of Zylon / Dyneema based material as an insulating material may reduce the frictional heat generated due to the wire motion.

No significant dependence of the voltage tap signal pattern and amplitude, duration of pulse width and energy dissipated due to wire motion was observed on wire current ramp rate.

Time duration of voltage spike is of the same order for all the samples used during the study. No significant dependence of time duration of voltage spike on wire current ramp rate and tension to the superconducting wire was observed.

Reversing the polarity of current in the superconducting wire erases the history and no significant effect on the electromagnetic force need to start the superconducting wire motion was observed. However, an asymmetric voltage signal pattern was observed presumably due to asymmetric position of superconducting wire in the semi-circular head.

A negative offset was observed during the measurements. The value and direction of offset is independent of current ramp rate, current direction in superconducting wire, tension to the superconducting wire and sample characteristics. The magnitude of offset voltage is ~ -3.0 E-04 V. The speculations are as follows; the thermoelectric voltage of voltage tap signal wire and the voltage induced due to mutual inductance between voltage tap loop wire and superconducting wire. The experimental results are repeatable under the same experimental conditions.

Zylon / Dyneema based materials can be used in superconducting magnets for practical applications. Superconducting coils wound on DFRP bobbins showed stable behavior in case of AC coils [37]. Dyneema random sheet can be placed / inserted between the coil layers and also as a spacer. Monofilament of Zylon / Dyneema can be wrapped in superconducting cables before wrapping with Polyimide film. Presently, punch through test and other electrical properties of Zylon / Dyneema based materials are not available. In view of this, we cannot replace Polyimide film with Zylon / Dyneema based materials, which is basically used as an insulating material. More study is to be carried out on Zylon / Dyneema based materials.

APPENDIX I

Formulation of thrust force exerted by superconducting wire to the semi-circular head

The superconducting wire is set on the semi-circular head and the tension T, provides a thrust force F_t (of the superconducting wire) against the semi-circular head as shown in fig. AI.1. The formulation of thrust force is estimated assuming head part as polygon and also a circle. Both the assumptions lead to same result. The formulations are described below.

1. **Formulation in case of polygon**

   Figure AI.2 shows the approximation of polygon having N spacers in a coil. Figure AI.3 shows the details of various parameters involved for calculations. The thrust force exerted by superconducting wire to one spacer is

$$F_{t1} = 2T \cdot Sin\left(\theta/2\right) = 2T \cdot Sin\left(2\pi/2N\right) = 2T \cdot Sin\left(\pi/N\right) \qquad \text{(AI.1)}$$

   where, T = tension of the superconducting wire.

   The thrust force exerted by superconducting wire to N spacers is

$$F_{tN} = N \times F_{t1} = 2N \cdot T \cdot Sin\left(\pi/N\right) \qquad \text{(AI.2)}$$

The thrust force per unit length of a spacer having width w is

$$\sigma_t = F_{t1}/w = \left(2T/w\right) \cdot Sin\left(\pi/N\right) \qquad \text{(AI.3)}$$

2. Formulation in case of circle

The thrust force exerted by superconductor in case of polygon can be approximated to circle if N → ∞. The thrust force by superconducting wire in case circle is

$$F_{(TotalCircumference)} = Lim_{(N\to\infty)} F_{tN} \tag{AI.4}$$

$$\begin{aligned} &Lim_{(N\to\infty)} F_{tN} = Lim_{(N\to\infty)} 2N \cdot T \cdot Sin\left(\pi/N\right) = \\ &2\pi T \cdot Lim_{(N\to\infty)}\left(N/\pi\right) \cdot Sin\left(\pi/N\right) \end{aligned} \tag{AI.5}$$

If we assume, $(\pi/N) = x$ (AI.6)

Then,

$$Lim_{(N\to\infty)} F_{tN} = 2\pi \cdot T \cdot Lim_{(x\to 0)}\left(1/x\right) \cdot Sinx \tag{AI.7}$$

$$Lim_{(x\to 0)}\left(1/x\right) \cdot Sinx = Lim_{(x\to 0)}\left(Sinx/x\right) = 1 \tag{AI.8}$$

Substituting (AI.8) into (AI.7) we got,

$$Lim_{(N\to\infty)} F_{tN} = 2\pi \cdot T \cdot Lim_{(x\to 0)}\left(1/x\right) \cdot Sinx = 2\pi \cdot T \tag{AI.9}$$

The compressive force to SC per unit length is

$$\sigma_{R(Circumference)} = F_{(TotalCircumference)} / 2\pi \cdot R = 2\pi \cdot T / 2\pi \cdot R = T/R \tag{AI.10}$$

Another approach is described in the following.

As above mentioned, F_t per unit length to a spacer in width w is shown in formula (AI.3).

$$\sigma_R = F_{t1}/w = \left(2T/w\right) \cdot Sin\left(\pi/N\right) \tag{AI.3}$$

When the circumference is covered all over with spacers, the width of spacer (w) is approximated to

$$w = \left(2\pi \cdot R \middle/ N\right) \tag{AI.11}$$

From formula (AI.3) and (AI.11), we get

$$\sigma_R = F_{R1} \middle/ w = \left(2T \cdot N \middle/ 2\pi \cdot R\right) \cdot Sin\left(\pi \middle/ N\right) = \left(T \cdot N \middle/ \pi \cdot R\right) \cdot Sin\left(\pi \middle/ N\right) \tag{AI.12}$$

In case of polygon to circle approximation (N$\rightarrow\infty$)

$$\sigma_{CircleR} = Lim_{(N\to\infty)}\sigma_R = Lim_{(N\to\infty)}\left(T \cdot N \middle/ \pi \cdot R\right) \cdot Sin\left(\pi \middle/ N\right) =$$
$$\left(T \middle/ R\right) Lim_{(N\to\infty)}\left(N \middle/ \pi\right) \cdot Sin\left(\pi \middle/ N\right)$$

$$\sigma_{CircleR} = T \middle/ R \tag{AI.13}$$

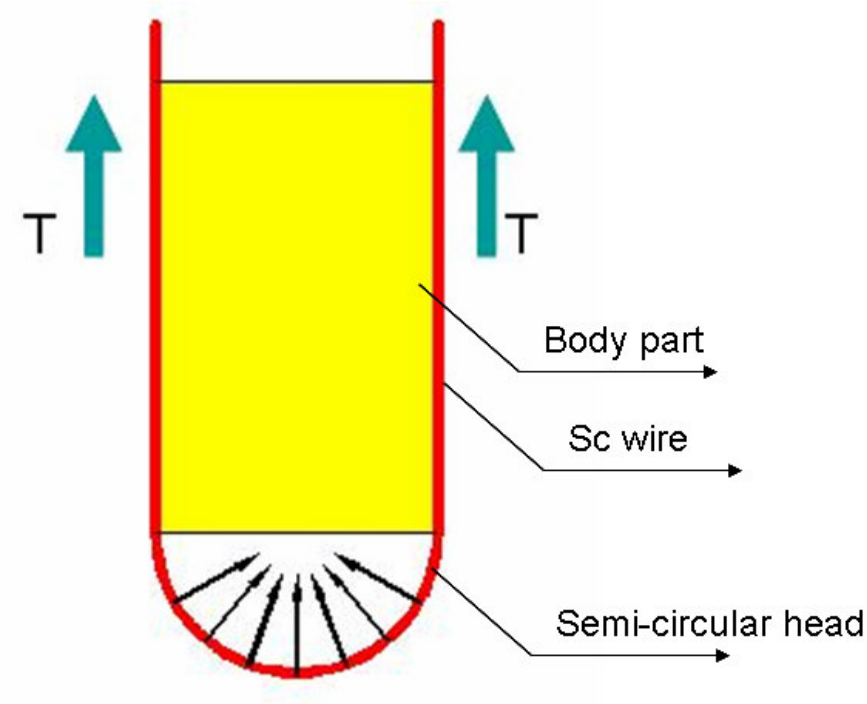

Figure AI.1: Thrust force applied by the superconducting wire to the semi-circular head.

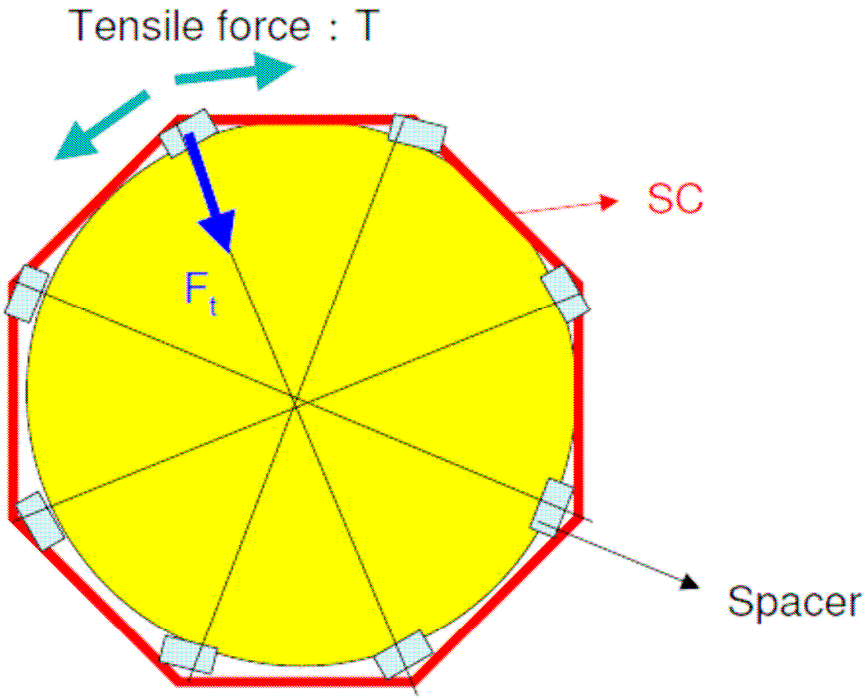

Figure AI.2: Approximation of polygon having N spacers.

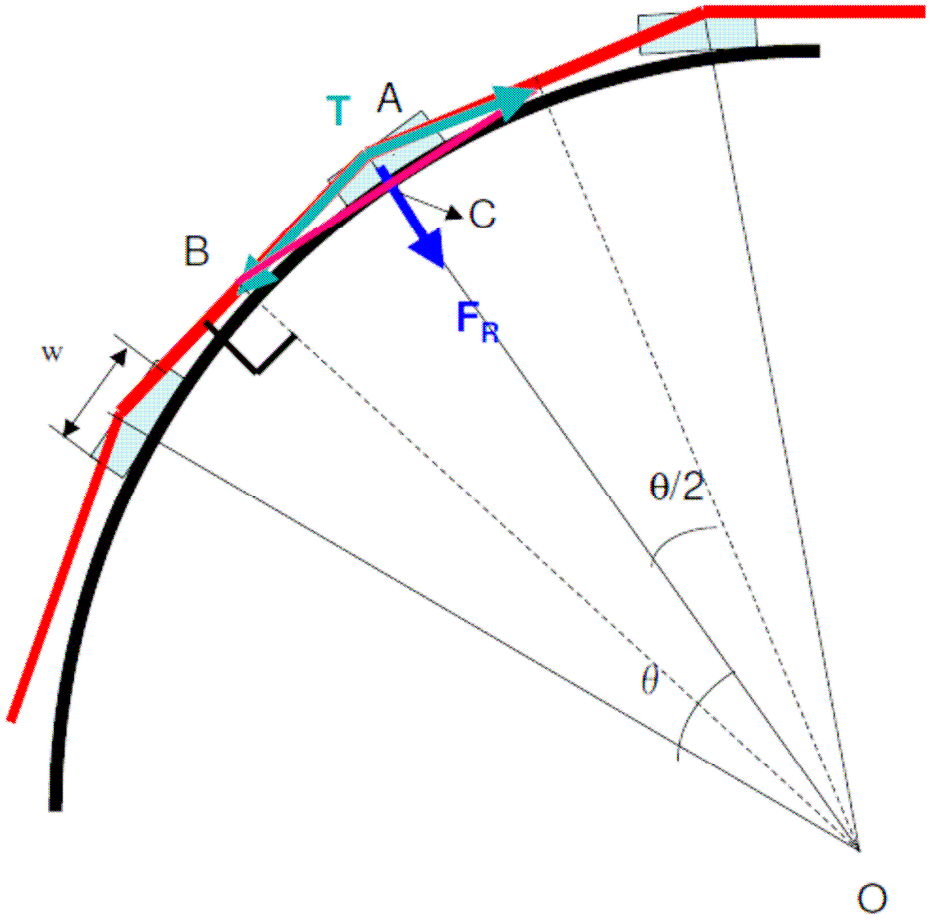

Figure AI.3: Detailed view of approximation of polygon having N spacers.

APPENDIX II

Formulation of velocity of wire motion, distance moved by wire and energy dissipation

In order to estimate the energy dissipated by the wire motion, we consider a wire of length dl carrying a current I in a magnetic flux density B. If the wire moves a distance dx as shown in fig. AII.1 during a time dt, a voltage V is induced along the wire. The induced voltage is given by

$$V = \frac{d\phi}{dt} = B \cdot dl \cdot \frac{dx}{dt} \qquad \text{(AII.1)}$$

On the other hand, the work of the Lorentz force F applied on the wire as

$$W = F \cdot dx \qquad \text{(AII.2)}$$

where, $F = B \cdot I \cdot dl$ (AII.3)

By combining eq. (AII.1), (AII.2) and (AII.3), it comes that the energy dissipated dE is

$$dE = I \cdot V \cdot dt \qquad \text{(AII.4)}$$

Integrating eq. (AII.4) over the duration of the wire motion gives the total energy E, released by the wire motions. In Eq. (AII.4), it is assumed that the conductor current remains constant during the motion. This assumption is valid because flux fluctuation due to conductor motion is negligible compared with the total flux.

Distance moved by wire and kinetic energy (Ke) released is estimated as follows:

Energy dissipated in moving a distance dx is given as

$$dE = F \cdot dx = I \cdot B \cdot dl \cdot dx$$

Voltage generated due to wire motion is given as

$$V = \frac{d\phi}{dt} = \frac{B \cdot da}{dt} = \frac{B \cdot dl \cdot v \cdot dt}{dt} = B \cdot v \cdot dl$$

Thus, velocity of wire motion is given by

$$v = \frac{dx}{dt} = \frac{V}{B \cdot dl} \qquad \text{(AII.5)}$$

where, dl = length of wire which moves under the Lorentz force (for calculation, we assumed 20 E-03 m).

dt = time to reach peak voltage.

Figure AII.2 shows the spike pattern and assuming linear rise of voltage spike (A to B), maximum velocity (at point B) is,

$$v_{max} = a * dt$$

Distance moved by a wire is

$$dx = \frac{1}{2} a * t^2 \qquad \text{(AII.6)}$$

We can write kinetic energy as

$$Ke = \frac{1}{2} m * v^2 \qquad \text{(AII.7)}$$

where, a = acceleration of wire motion.

m = mass of wire.

t = total time duration of voltage pulse.

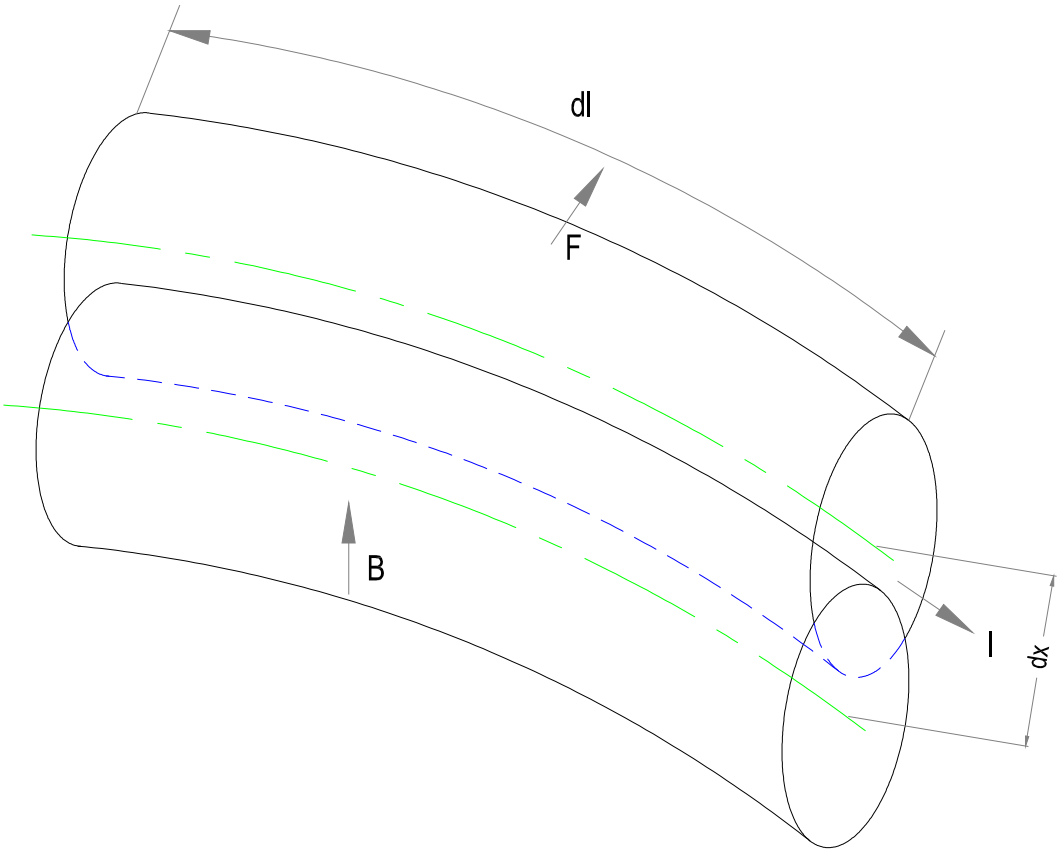

Figure AII.1: Conceptual view of wire carrying current and moves a distance *dx* in magnetic field.

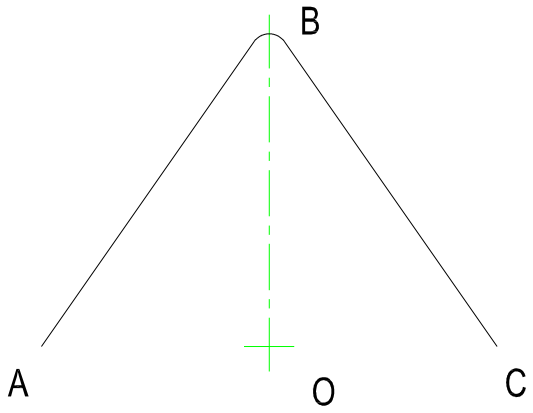

Figure AII.2: Spike pattern with linear rise and fall.

Bibliography

1. A. Yamanaka, T. Kashima, S. Nago, K. Hosoyama, T. Takao, S. Sato, and M. Takeo, Physica C 372-376, 2002, 1447.
2. T. Kashima, A. Yamanaka, S. Takasugi, and S. Nishihara, Adv. Cryog Eng. 46, 2000, 329.
3. T. Takao, T. Nemoto, H. Konda, T. Kashima, and A. Yamanaka, ICECE16/ICMC, ICMC, 1997, 1993.
4. Maddock B J, James G B and Norris W T, Cryogenics, 9, 1969, 261.
5. Maddock B J and James GB, Proc. IEE 115, 1968, 543.
6. Stekly Z J J 1967 Proc. Cony. oii Ititetise .Magtietic Fields, Grenoble (Paris: CNRS) p 237).
7. Appleton AD and MacNab RB 1970 Proc. 3rd In/. Crjogenic Eng. Cotif., Berlin.
8. Purcell J R I968 Proc. Summer Study on Superconducting Devices, Brookhaven, US Dept of Commerce report BNL 50155 (C-55) p 765.
9. M.N. Wilson, Superconducting Magnets, Oxford University Press; 1986.
10. N.Yanagi, K. Seo, S. Imagawa, H. Sekiguchi, K. Takahata, S. Yamada, T. Mito, T. Ishigohka, A. Ninomiya, Fusion Engineering and Design 81 (2006) 2561.
11. Y. Iwasa, Proceedings of the Workshop on Stability of Superconductors in Helium I and II, Saclay, France, November 16-19, 1981, pp. 125, edited by Institu International du froid (Commision A1/2), Paris, France;
12. A. Devred, US Particle Accelerator School, Upton, NY, USA, July 29-August 4, 1990.
13. T. Ogitsu, K. Tsuchiya and A. Devred, IEEE Trans. On Mag., Vol. 27 (2),1991, 2132.
14. R.S. Kensley and Y. Iwasa, Cryogenics January 1980, 25.
15. A. Devred, CAS-CERN Proc. 98-05.
16. Ramesh Gupta, Lecture notes of School on Superconductivity, Cryogenics Application and Technology, CAT, Indore, India, 1998.

17. H. Maeda, O. Tsukamoto, Y. Iwasa, Proc. of 9th International Cryogenic Engineering Conference, Kobe, Japan, 1982, 543.
18. O. Tsukamoto, H. Maeda, Y. Iwasa, Appl. Phys. Lett., 39, 1981, 918.
19. T. Yamada, M. Iwamoto, H. Sakamoto, M. Morita, Y. Jizo, S. Karino, IEEE Trans. On Mag., 17(5), 1981, 1799.
20. K. Tsuchiya, K. Hosoyama, Y. Ajima, K. Egawa, N. Kumagai, S. Mitsunobu, Y. Sakakibara, A. Terashima, T. Ogitsu, Ad. Cryo. Eng. 31, 1986, 173.
21. S. Nishijima, T. Kushida, T. Okada, S. Namba, IEEE Trans. On App. Supercond., Vol. 7, No. 2 (1997), 163.
22. H. Shimizu, T. Shiroki, Y okomizu, IEEE Trans. On Appl. Supercond. 10(1), 2000, 689.
23. J. Perot. Special Magnets. CAS - Superconductivity in Particle Accelerators, 1996. CERN 96-03.24.
24. K. Ruwali, A. Yamanaka, Y. Teramoto, K. Nakanishi and K. Hosoyama, in Proceedings of the 11th European Particle Accelerator Conference, Genoa, 2008 (EPS-AG, Genoa, Italy, 2008), p. 2449.
25. K. Ruwali, A. Yamanaka, Y. Teramoto, K. Nakanishi and K. Hosoyama, Phys. Rev. ST Accel. Beams 12, 042401 (2009).
26. A. Devred, CAS-CERN 98-05.
27. R.A. Haarman and K.D. Williamson, Jr., Electrical Breakdown and tracking characteristics of pulsed high voltages in cryogenic helium and nitrogen, Advances in Cryogenic Engineering, 21: 102–108, 1975.
28. Toyobo Co., Ltd., http://www.toyobo.co.jp/e/seihin/dn/dyneema/ index.htm.
29. T. Kashima et al, Advances in Cryogenics Engineering, Vol. 42, 1996, 147.
30. T. Takao, T. Nemoto, H. Konda, T. Kashima and A. Yamanaka, ICECE16/ICMC, ICMC, 1997, 1993.
31. H. Fujishiro et al, Jpn. J. Appl. Phys. Vol. 36, 1997, 5633.
32. Department of Zylon, Toyobo Co., Ltd. Home page, Osaka. Available from http://www.toyobo.co.jp/e/seihin/ke/pbo/index.htm.
33. T. Kuroki, K. Yabuki, “Physical properties and application of PBO fiber Zylon”, Sen`I gakkaishi, vol. 54, no. 1, pp. 16-20 (1998) (in Japanese).

34. T. Takao, T. Kashima, A. Yamanaka, “Frictional properties on surfaces of high strength polymer fiber reinforced plastics”, Adv. in Cryog. Eng., 2000, 46A, 127.
35. S.B. Ainbinder and L.M. Liberman, Mechanics of Composite Materials, Vol. 9, No. 5, 1973, 825.
36. Y. Iwasa, I.I.F.-I.I.R.-Commission A1/2 Scalay (France) 1981/6.
37. T. Kashima, A. Yamanaka, E. S. Yoneda, S. Nishijima, T. Okada, Adv. Cryog. Eng. 41 (1996) 441.